THE ASTROPHYSICAL JOURNAL SUPPLEMENT SERIES, 72:231–244, 1990 February

SEYFERT GALAXIES. I. MORPHOLOGIES, MAGNITUDES, AND DISKS

JOHN W. MACKENTY
Institute for Astronomy, University of Hawaii, and Space Telescope Science Institute
Received 1987 March 18; accepted 1989 July 31

ABSTRACT

CCD images of a volume- and luminosity-limited sample of 51 Markarian and NGC Seyfert galaxies show that Seyfert galaxies nearly always possess mechanisms for transporting material into their nuclei (e.g., peculiar, tidally interacting, or barred galaxies). A subset of Seyfert galaxies with amorphous morphologies, some of which may be remnants of past interactions, constitutes approximately one-fifth of the sample. The colors and exponential disk parameters of Seyfert galaxies are generally similar to those of spiral galaxies without active nuclei. Images of the galaxies are presented along with aperture magnitudes.

Subject headings: galaxies: nuclei — galaxies: photometry — galaxies: Seyfert — galaxies: structure

I. INTRODUCTION

This paper examines the morphologies and colors of Seyfert galaxies. The primary motivation is to extend the efforts of earlier authors through the use of the charge-coupled device (CCD) detector and by compiling an improved sample of Seyfert galaxies.

In a classic study of the morphology of Seyfert galaxies, Adams (1977) found that nearly all Seyferts have spiral or barred spiral or barred spiral morphologies. Several galaxies were classed as possible ellipticals, but in no case was any member of the sample clearly an elliptical galaxy. Adams (1977) also noted that "there is apparently a surplus of Seyfert nuclei in disturbed and interacting systems." Adams's survey consisted of image-tube plates of 60 galaxies; together with published material on 20 additional galaxies, it encompassed nearly all of the then-recognized Seyfert galaxies. In a prescient paper, Kalloglian (1971) noted the frequent occurrence of peculiar morphologies and bars in Markarian galaxies and concluded that their "spectra depends on the morphological type of the galaxies." Wehinger and Wyckoff (1977) examined 12 high-redshift Seyfert galaxies with an electronographic camera. These galaxies are generally more luminous than those included in the survey of Adams (1977). Wehinger and Wyckoff (1977) found 60% to be spirals and most of the remainder to have "jets or other distrubed features." From a photographic study of 30 Seyfert galaxies with redshifts less than 5000 km s^{-1}, Simkin, Su, and Schwarz (1980) proposed an evolutionary scheme in which gas is supplied to the nucleus, and signs of that process become evident in ringlike structures in the disk of the galaxy. Three-color surface photometry has been obtained for 20 Seyfert galaxies by Yee (1983). Despite the difficulties posed by the limited dynamic range of the SIT camera used in his study, Yee found that the disk parameters and colors of Seyfert galaxies are similar to those of normal spiral galaxies, with the exception of a possibly higher central surface brightness in the Seyfert disks.

Single-beam H I (21 cm) observations also provide information on the structure and kinematics of Seyfert galaxies. Heckman, Balick, and Sullivan (1978) find approximately one-third of a sample of 58 Seyfert and "Seyfert-like" galaxies have "strong anomalies" in their H I spectra. A larger survey of 91 Seyferts by Mirabel and Wilson (1984) shows 40% with peculiarities attributed to either close companions in the telescope beam or tidal interactions that have perturbed the neutral gas in the galaxies.

Somewhat surprisingly, much of the progress in recent years toward an understanding of the host galaxies of AGNs comes from studies of low-redshift QSOs. This was sparked in part by the debate over the true distances of QSOs. Stockton (1978) demonstrated that QSOs do have cosmological redshifts and seem to prefer to reside in small groups of galaxies. Hutchings *et al.* (1981, 1982), Hutchings, Crampton, and Campbell (1984), Wyckoff, Wehinger, and Gehren (1981), and Malkan, Margon, and Chanan (1984) have detected faint "fuzz" underlying most of the low-redshift QSOs and have shown that this nebulosity has the correct colors, magnitudes, and scale lengths for galaxies at the redshift of the resident QSO nuclei. Boroson and Oke (1982), MacKenty and Stockton (1984), Boroson, Persson, and Oke (1985), and Heckman *et al.* (1984) have succeeded in obtaining spectra of several QSO host galaxies that show stellar absorption lines at the same redshift as the QSO nuclei.

Gunn (1979) suggested that a means of supplying the nucleus of an active galaxy with "fuel" might be interactions with neighboring galaxies. Stockton (1982) noted the presence of very close (and probably tidally truncated) companions near several QSOs and proposed that interactions are a means by which the central massive objects (in current-epoch AGNs) are supplied with gas. Fosbury *et al.* (1982) and Stauffer (1982) also discussed the putative role of tidal interactions in fueling radio galaxies and emission-line galaxies with nonthermal continua, respectively.

Images and spectra of the host galaxies of the low-redshift QSOs tend to support this concept. Hutchings, Crampton, and Campbell (1984) find that one-third of their sample (78 galaxies) appears to be interacting and that one-fourth is in compact groups or clusters of galaxies. Spectra of the low-redshift QSOs 3C 48 (Boroson and Oke 1982) and Markarian 1014 (MacKenty and Stockton 1984) show Balmer line ab-

sorption in the host galaxies, indicating a recent episode of star formation; furthermore, Markarian 1014's morphology is quite asymmetric. Photoionized gas structures suggestive of tidal features have been discovered associated with luminous low-redshift QSOs (Stockton and MacKenty 1983, 1986). Keel (1985) and MacKenty (1986) report Seyfert galaxies with tidal tails.

Following the initial suggestions of Toomre and Toomre (1972) and Gunn (1979), the theoretical consequences of galaxy mergers and interactions on active galaxies have been considered by several authors. Norman and Silk (1983) note that any general distortion in the central region of the galaxy would suffice to increase the input of "fuel" to the nucleus and suggest that such distortions might arise from mergers, bars, or infall of gas clouds. de Robertis (1985) finds the behavior of the QSO luminosity function consistent with observations in a scenario where galaxy interactions trigger nuclear activity. Roos (1981, 1985*a*, *b*) and Gaskell (1985) have considered the possibility that the interacting galaxies actually responsible for the activity are rather small galaxies.

A volume- and luminosity-limited sample of Seyfert galaxies is defined in § II, and its completeness is compared to the samples used in previous morphological surveys. CCD observations of this sample are described in § III, and their analysis is explained in § IV. The system devised for classifying the morphologies of the galaxies in the survey and notes on selected galaxies are presented in § V. The results are discussed in § VI, and the conclusions are summarized in § VII.

II. SELECTION OF THE SAMPLE

Any survey of Seyfert galaxies must take into account the difficulties inherent in their discovery. It is interesting to note that ~ 3000 QSOs have been cataloged (Hewitt and Burbidge 1980; Veron-Cetty and Veron 1984), while only 200–300 Seyfert galaxies are known. The relatively small number of cataloged Seyfert galaxies is primarily the result of the methods used in the discovery of Seyfert galaxies. Two methods have accounted for most of the currently cataloged Seyfert galaxies: surveys of UV-excess objects and direct spectroscopy. Weedman (1977), Balick and Heckman (1982*a*), Huchra, Wyatt, and Davis (1982), and Osterbrock (1984) have recently reviewed the methods of discovery of Seyfert galaxies and some of the associated selection effects.

For the present study, the three critical constraints are (1) the maximum distances, (2) the minimum absolute luminosities, and (3) the minimum apparent brightnesses of the galaxies to be included in the sample. The limiting distance is directly coupled to the spatial resolution or scale that is achievable for the most distant objects. By selecting rather luminous Seyfert galaxies, the sample is closely akin to the more luminous QSOs and is clearly distinct from galaxies with LINER (Heckman 1980*a*) or starburst characteristics (Balzano 1983). And, since most catalogs of astronomical objects are flux limited, the apparent magnitude constraint must be chosen to be in accord with the limiting apparent magnitude of the available catalogs.

All distance measures and absolute luminosties in this paper assume $H_0 = 75$ km s^{-1} Mpc^{-1}, $q_0 = 0.5$. When distances or magnitudes taken from other works are cited, it should be understood that the values have been converted to this cosmology when necessary.

Markarian and his coworkers (Markarian 1967; Markarian, Lipovetskii, and Stepanian 1979) have compiled the largest catalog of Seyfert galaxies during their search for UV-excess galaxies. From 1967 to 1979 they published 15 lists containing 1500 galaxies. The Markarian UV-excess survey becomes increasingly incomplete for galaxies of apparent magnitude fainter than $\sim 15.5 m_{pg}$ (Huchra and Sargent 1973; Meurs and Wilson 1984). Furthermore, the Markarian lists exclude galaxies brighter than $\sim 13 m_{pg}$ (Markarian 1967). However, a significant number of bright galaxies from the Revised New General Catalog (RNGC; Sulentic and Tifft 1973) are known (from a variety of discovery methods) to be Seyfert galaxies.

Schinckel and Phillips (1982) have compiled a catalog from the published literature (and a few observations of their own) that contains all identified Seyfert galaxies and, in addition, many galaxies identified as having LINER spectra. From their catalog, all Seyfert galaxies that are (1) included in the Markarian or NGC catalogs, (2) have declinations between $-20°$ and $+60°$, (3) have redshifts between 3000 and 13,000 km s^{-1}, (4) have absolute magnitudes less than $-19 M_{pg}$, and (5) have apparent magnitudes less than $16.5 m_{pg}$ are included in the present sample. These constraints were chosen to produce as complete a sample as possible and still retain a sufficiently large number of galaxies on which to perform a statistical analysis. A sample of ~ 50 galaxies both satisfied these requirements and was reasonable in terms of the available telescope time.

The 51 Seyfert galaxies selected for this study are listed in Table 1, columns (1) and (2). A plot of their absolute magnitudes in V (for 30 kpc apertures) versus redshift is shown in Figure 1 (the magnitudes, obtained here, are ~1 mag brighter than Markarian's). The absence of galaxies in the upper right region of this figure reflects the incompleteness of the Markarian survey. The median redshift of the sample is 9450 km s^{-1}.

The selection of the sample was made in 1983 September, based on the data available at that time. The only magnitudes then available for the entire sample (excluding the brighter NGC galaxies) are those from the Markarian lists which are known to be uncertain to ~ 0.5 mag. The most important consideration in constructing this catalog was to avoid bias related to the morphologies of the Seyfert galaxies. Since only a fraction (consisting mainly of the most studied and perhaps the more "interesting") of the Markarian Seyfert galaxies have published magnitudes of significantly greater accuracy than Markarian's, in constructing the sample the Markarian magnitudes were used for all Markarian galaxies, and the RNGC magnitudes were used for the seven NGC galaxies not included in the Markarian lists. The same reasoning applies to the decision to select galaxies based on their total magnitudes rather than on their nuclear magnitudes. To have selected the sample based on, for example, [O III] fluxes, might have added more severe biases. Keel (1980) and Lawrence and Elvis (1982) have discussed the connection between the inclination of an active galaxy and its nuclear spectrum. Overall, it seems preferable to keep the sample selection criteria closely coupled to Markarian's discovery data since this sample is in-

TABLE 1

PROPERTIES OF THE SAMPLE

	(1)	(2)	(3)	(4)	(5)	(6)	(7)	(8)	(9)	(10)	(11)	(12)	(13)	(14)
Name	Mrk	NGC	z	Type	m_{pg} (Mrk)	B II	Night	Seeing	Resolution	MC	IC	PA	a	b/a
0004+200	335	...	7500	1	14.0	-41.4	20	1.0	0.48	0	0	...	3.1	1.00
0045+143	1146	...	11850	1	15.5	-48.2	19	1.1	0.78	2	0	73	9.9	0.70
0204-003	1018	...	12810	1	14.0	-57.7	20	1.1	0.86	3	0	175	12.3	0.61
0212-010	590	863	8100	1.5	14.5	-56.9	20	1.2	0.58	1	1	135	12.4	0.84
0225+311	1040	931	4910	1.5	15.0	-27.2	23	4.0	1.23	1	2	75	16.8	0.25
0228-091	1044	...	4920	1	14.5	-60.5	23	4.2	1.30	2	0	81	4.0	0.78
0232-090	1048	985	12950	1.5	14.5	-59.5	23	3.9	3.03	3	0	69	16.0	0.84
0236+014	...	1019	7251	1	14.5	-51.2	23	3.4	1.51	2	2	35	9.6	0.77
0239+070	595	...	8400	1	16.0	-46.5	23	3.8	1.94	0	0	101	6.4	0.74
0247+191	372	...	9300	1.5	15.5	-35.5	23	4.5	2.58	0(1)	0	159	6.9	0.81
0323-062	609	...	9600	1.8	14.5	-47.8	23	3.5	2.07	0	2	...	6.7	0.98
0328-032	612	...	6066	2	15.5	-45.0	23	4.0	1.51	2	3	131	6.9	0.61
0331-052	0	1358	4071	2	12.5	-45.6	23	4.5	1.16	2	1	5	11.5	0.78
0339-013	0	1409	7380	2	14.0	-41.8	23	5.6	2.58	3	3	33	12.6	0.59
0434-103	618	...	10200	1	14.5	-34.7	23	4.0	2.48	2	2	165	11.5	0.47
0446-062	0	1667	4578	2	13.0	-30.1	23	3.5	1.01	1	1(3)	165	10.0	0.78
0514-001	1095	...	9900	1	14.5	-21.1	23	3.4	2.04	3	0	17	9.0	0.86
0733+585	9	...	12040	1	14.5	28.7	23	2.8	2.04	3	0	...	8.6	0.95
0739+500	79	...	6580	1.2	13.5	28.4	30	2.9	1.19	2(3)	0	65	10.2	0.60
0752+392	382	...	10200	1	15.5	28.6	30	2.6	1.62	2	0	9	6.7	0.69
0804+391	622	...	6925	2	15.0	30.8	30	3.1	1.33	0	1	...	5.1	0.90
0916+163	704	...	8930	1	15.0	39.7	30	2.8	1.52	1(2)	1	73	6.6	0.57
0922+523	110	...	10800	1	16.0	44.4	30	2.8	1.82	3	0	...	4.2	1.00
1124+353	423	...	9720	1.9	15.5	70.2	30	2.6	1.55	3	3	9	7.2	0.85
1202+204	...	4074	6600	2	15.5	77.3	30	2.3	0.96	0(1)	0	105	5.8	0.64
1207+472	198	...	7220	2	15.0	68.4	13	1.7	0.77	1	0	35	6.1	0.73
1216+301	766	4253	3850	1	14.0	82.3	13	1.6	0.38	2(3)	0	69	5.1	0.89
1221+030	50	...	6910	1	15.5	64.6	30	2.1	0.92	0(3)	0	170	4.1	0.76
1254+571	231	...	12300	1	14.0	60.2	13	1.6	1.18	3	0	35	10.3	0.85
1339+304	268	...	12300	2	15.0	78.6	13	2.2	1.64	0(1)	2	115	11.9	0.59
1343+561	273	...	11400	2	14.5	59.7	30	2.1	1.43	3	0(1)	3	8.3	0.69
1416+252	...	5548	4990	1.5	13.5	70.5	30	2.0	0.62	3	0	127	6.8	0.75
1433+485	474	5683	12300	1	16.5	60.6	30	2.0	1.47	2	0	...	6.4	0.86
1435+590	817	...	9450	1	14.0	53.5	30	1.9	1.09	0(3)	0	...	7.5	0.92
1439+534	477	...	11220	2	16.0	56.8	...	...	...	0	3	...	...	...
1502+104	841	...	10930	1.2	14.0	54.6	20	1.6	1.05	0	0	...	5.1	0.95
1535+580	290	...	9240	1	15.0	48.0	13	1.4	0.81	0	0	...	4.3	1.00
1535+544	486	...	11700	1	15.0	49.4	13	1.5	1.07	3	1	144	4.8	0.54
1553+192	291	...	10500	1	15.0	47.3	13	1.4	0.88	2	0	35	5.8	0.55
1557+351	493	...	9900	1	16.0	49.4	13	1.5	0.88	2	0	55	9.9	0.65
1606+123	871	...	9980	1	15.0	41.6	13	1.6	0.95	1(2)	0	107	10.3	0.52
1622+411	699	...	10110	1	16.5	44.6	13	1.3	0.81	0	1	...	...	...
1721+310	506	...	12981	1.5	15.5	31.5	13	1.3	1.04	2	2	119	10.9	0.74
2041-105	509	...	10650	1	13.0	-29.9	13	1.4	0.91	0	0	...	6.1	0.96
2154+071	516	...	8545	1	16.0	-35.4	13	1.3	0.7	1(2)	0	81	5.5	0.69
2301+084	...	7469	5020	1	13.5	-45.5	...	...	...	1	2	...	...	...
2302+222	315	...	11830	1.5	15.0	-33.9	13	1.3	0.96	1(3)	0	59	6.5	0.86
2316-000	530	7603	8800	1.5	14.5	-54.7	19	1.4	0.75	3	0	165	14.5	0.65
2325+083	533	7674	8620	2	16.0	-48.8	13	1.4	0.73	3	3	155	13.9	0.66
2353+071	541	...	12300	1	15.5	-52.8	19	1.2	0.87	1(2)	0	173	7.0	0.72
2359+030	543	7811	7800	1	15.5	-57.3	20	1.3	0.63	1	0	...	6.2	0.94

TABLE 1—*Continued*

(15)	(16)	(17)	(18)	(19)	(20)	(21)	(22)	(23)	(24)	(25)	(26)	(27)	(28)	(29)	(30)
	30 kpc Aperture			5 kpc Aperture			5-10 kpc Annulus			Central S.B.			Disk Fraction		
r_0	V	B-V	V-R	V	B-V	V-R	V	B-V	V-R	B	V	R	B	V	R
2.58	-21.46	0.22	0.45	-21.35	0.22	0.46	-18.18	0.86	0.26	22.5	21.5	21.5	0.06	0.13	0.08
4.23	-21.36	0.90	0.63	-20.06	0.80	0.71	-20.23	0.95	0.60	21.3	20.4	19.9	0.85	0.83	0.76
5.72	-22.17	0.94	0.59	-21.19	0.84	0.64	-20.79	1.00	0.55	22.2	21.2	20.6	0.41	0.41	0.43
6.14	-22.05	0.87	0.57	-20.89	0.96	0.65	-20.70	0.83	0.52	21.6	20.8	20.3	0.64	0.60	0.56
10.88[a]	-20.91	0.72	0.63	-19.55	0.76	0.69	-19.62	0.66	0.64	...	...	...	...	...	...
3.04	-20.14	0.24	0.55	-19.73	0.22	0.48	-17.98	0.41	0.60	21.7	21.4	20.6	0.37	0.41	0.49
4.97	-22.09	0.46	0.53	-20.97	0.33	0.55	-20.54	0.64	0.53	20.1	19.5	19.0	...	...	...
5.49:	-21.07	0.55	0.53	-19.57	0.54	0.60	-19.99	0.52	0.51	22.2	21.9	21.4	0.56	0.44	0.43
4.06	-20.81	0.69	0.60	-20.12	0.43	0.65	-18.98	1.15	0.59	23.3	21.6	20.9	0.18	0.44	0.46
2.53	-20.81	0.82	0.60	-19.75	0.66	0.68	-19.38	0.91	0.52	21.4	20.5	19.7	0.56	0.62	0.74
4.95	-21.55	0.40	0.55	-20.91	0.31	0.56	-19.49	0.54	0.55	23.5	22.4	21.4	0.09	0.16	0.25
3.41	-20.61	0.66	0.55	-19.89	0.69	0.50	-18.73	0.56	0.64	22.9	22.0	21.4	0.29	0.35	0.39
17.02[b]	-21.31	0.67	0.53	-20.10	0.76	0.52	-19.87	0.67	0.53	...	...	...	...	...	...
7.79	-21.45	0.85	0.65	-19.92	1.00	0.58	-20.46	0.79	0.64	22.6	21.7	21.0	0.42	0.45	0.44
4.22[a]	-21.62	0.34	0.52	-20.57	0.24	0.41	-20.29	0.45	0.56	...	...	...	...	...	...
5.31	-21.66	0.48	0.55	-20.27	0.60	0.56	-20.54	0.40	0.53	21.8	21.1	20.7	0.33	0.39	0.34
7.63	-22.26	0.21	0.58	-21.82	0.08	0.51	-19.99	0.60	0.66	22.8	22.0	21.3	0.12	0.21	0.24
3.34	-21.70	0.36	0.53	-20.93	0.21	0.55	-20.11	0.67	0.51	21.2	20.4	19.8	0.35	0.50	0.51
6.60	-21.38	0.39	0.96	-20.50	0.17	0.98	-19.90	0.55	0.96	22.1	21.5	20.6	0.41	0.51	0.50
5.10	-21.12	0.59	0.43	-20.11	0.56	0.45	-19.75	0.56	0.41	22.0	21.5	21.1	0.70	0.67	0.00
1.56	-20.58	0.67	0.53	-20.07	0.68	0.51	-18.54	0.58	0.60	19.5	19.3	18.4	...	...	...
3.56	-21.34	0.63	0.60	-20.85	0.48	0.62	-19.41	0.95	0.51	23.3	22.1	21.6	0.13	0.22	0.21
6.85	-21.37	0.44	0.54	-20.78	0.32	0.59	-19.20	0.72	0.47	23.5	22.9	22.5	0.17	0.19	0.00
3.58	-21.55	0.72	0.53	-20.69	0.77	0.57	-20.12	0.69	0.51	21.3	20.6	20.2	0.53	0.50	0.46
3.92	-20.67	0.99	0.58	-19.98	1.02	0.61	-18.85	0.99	0.57	22.4	21.5	20.9	0.48	0.45	0.45
3.41	-20.80	0.79	0.58	-20.11	0.78	0.59	-19.23	0.82	0.57	21.5	20.6	20.0	0.59	0.65	0.65
2.07	-20.58	0.75	0.55	-20.00	0.70	0.57	-18.50	0.87	0.47	21.4	20.4	20.0	0.40	0.50	0.44
3.84	-20.14	0.73	0.55	-19.58	0.68	0.58	-18.06	0.80	0.51	23.5	22.7	22.0	0.26	0.28	0.33
4.37	-22.87	0.75	0.56	-22.46	0.80	0.57	-20.71	0.64	0.54	20.8	20.2	19.6	0.35	0.32	0.31
3.89	-21.88	0.88	0.61	-20.91	0.97	0.66	-20.40	0.76	0.56	20.2	19.5	18.8	...	...	...
13.00[c]	-21.59	0.84	0.53	-20.44	0.88	0.69	-20.08	0.77	0.43	...	...	...	...	...	...
3.80	-21.55	0.64	0.57	-20.74	0.47	0.67	-19.94	0.80	0.46	20.9	20.0	19.6	0.64	0.00	0.69
2.84	-21.14	0.88	0.56	-20.22	0.87	0.65	-19.73	0.84	0.48	21.2	20.3	19.9	0.67	0.70	0.59
2.50	-21.74	0.57	0.50	-20.99	0.38	0.55	-20.13	0.84	0.45	20.4	19.4	19.1	0.46	0.66	0.00
...	...	...	...	...	...	...	...	...	...	...	...	...	...	...	...
5.65	-21.85	0.27	0.52	-21.64	0.21	0.50	-19.07	0.63	0.52	23.2	22.4	22.4	0.10	0.15	0.09
3.74	-21.01	0.48	0.56	-20.70	0.36	0.56	-18.49	0.97	0.57	23.2	22.4	21.6	0.13	0.16	0.21
9.06[c]	-21.39	0.42	0.58	-21.29	0.41	0.59	-17.65	0.80	0.51	...	...	...	...	...	...
2.97:	-20.57	0.70	0.41	-19.91	0.58	0.46	-18.65	0.72	0.39	21.8	20.9	20.7	0.43	0.53	0.43
6.92:	-21.34	0.72	0.54	-20.16	0.63	0.56	-20.25	0.75	0.51	22.2	21.3	20.8	0.58	0.65	0.65
3.36	-21.38	0.74	0.56	-20.42	0.78	0.60	-20.07	0.70	0.52	20.2	19.5	19.0	...	...	...
...	...	...	...	...	...	...	...	...	...	...	...	...	...	...	...
6.60	-21.88	0.90	0.59	-20.68	0.80	0.58	-20.76	0.98	0.60	22.0	21.0	20.5	0.49	0.54	0.51
3.57	-22.71	0.30	0.58	-22.53	0.26	0.57	-19.61	0.66	0.66	21.4	20.6	20.0	0.12	0.17	0.18
2.55	-20.58	0.85	0.59	-19.96	0.87	0.63	-18.49	0.71	0.54	22.8	21.6	21.0	0.21	0.28	0.28
...	...	...	...	...	...	...	...	...	...	...	...	...	...	...	...
5.29	-21.49	0.89	0.64	-20.61	0.88	0.69	-19.76	0.96	0.58	23.2	22.1	21.7	0.20	0.27	0.22
6.01	-22.22	0.78	0.60	-21.14	0.57	0.62	-20.87	0.93	0.57	23.1	22.1	21.6	0.24	0.30	0.27
5.28	-22.05	0.76	0.50	-20.55	1.08	0.44	-20.95	0.65	0.51	20.6	20.0	19.5	0.93	0.85	0.85
5.22	-21.34	0.91	0.63	-20.47	0.90	0.68	-19.67	0.93	0.57	21.9	20.9	20.3	0.64	0.69	0.67
4.39	-21.21	0.67	0.47	-20.24	0.70	0.51	-19.53	0.72	0.44	22.7	22.0	21.5	0.25	0.25	0.27

NOTES.—Key to column headings is as follows: col. (1) Markarian name; col. (2) NGC name; col. (3) redshift in km s^{-1}; col. (4) Seyfert type; col. (5) m_{pg}, from Markarian; col. (6) Galactic latitude; col. (7) night of photometric observations; col. (8) mean seeing in arc seconds of the B, V, and R photometric observations; col. (9) same as col. (8) expressed in kiloparsecs; col. (10) morphological class with alternate classification in parentheses; col. (11) interaction class; col. (12) position angle of the 24th R mag isophote; col. (13) semimajor axes length in kiloparsecs; col. (14) ratio of the minor and major axis length of the 24th R mag isophote; col. (15) exponential disk scale length in kiloparsecs; cols. (16)–(18) V, $B-V$, and $V-R$ magnitude and colors in 30 kpc diameter apertures; cols. (19)–(21) same as cols. (16)–(18) for 5 kpc diameter apertures; cols. (22)–(24) same as cols. (16)–(18) for an annulus between 5 and 10 kpc in radius; cols. (25)–(27) the B, V, and R central surface brightnesses (not corrected for inclination); cols. (28)–(30) the fraction of the luminosity within 32 kpc contained in the exponential disk component.

[a] Highly inclined.

[b] No obvious disk.

[c] Peculiar profile.

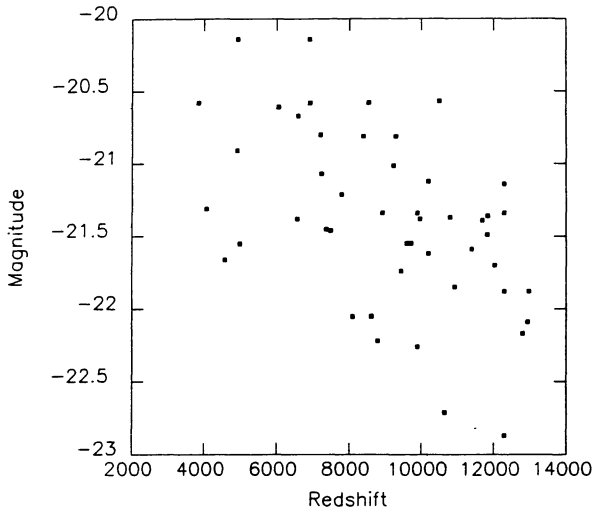

FIG. 1.—The absolute magnitudes in V (in 30 kpc diameter apertures) vs. redshift. Some incompleteness is evident in the upper right corner.

tended primarily to study Markarian Seyfert galaxies. New magnitudes for all of these galaxies, derived from the images obtained for this survey, are presented in this paper.

If the lower redshift limit of 3000 km s^{-1} were removed, the sample as defined above would contain five additional galaxies: NGC 1068 (1090 km s^{-1}), NGC 4151 (990 km s^{-1}), NGC 4258 (537 km s^{-1}), NGC 4388 (2450 km s^{-1}), and NGC 5728 (2970 km s^{-1}). Although these galaxies were observed, the subtraction of the night sky from the images of these galaxies proved to be rather unreliable.

Huchra and Sargent (1973) applied the $\langle V/V(\max)\rangle$ test to the first four Markarian lists (401 galaxies, for which they had redshifts of 332) and found increasing and significant incompleteness for galaxies fainter than $m_{pg} \sim 15.5$. Meurs and Wilson (1984) reached similar conclusions about the Markarian survey. The results of a $\langle V/V(\max)\rangle$ test (using Markarian's magnitudes where possible and including the five galaxies with velocities less than 3000 km s^{-1}) on the Seyfert sample selected for this paper indicate that the sample is virtually complete for the 85% of the galaxies brighter than $15.5 m_{pg}$.

The incompleteness at faint magnitudes appears to be inescapable at the present time in any Seyfert sample of the order of 50 galaxies. The *IRAS* data base may yield an equally good or perhaps superior sample of Seyfert galaxies (see de Grip *et al.* 1985), although *IRAS*-selected Seyfert galaxies may represent a different class of Seyfert galaxies than "classical" Markarian Seyfert galaxies. While it is perhaps debatable which method of discovering Seyfert galaxies is best, galaxies with photoionized broad- and narrow-line regions reflect the majority of that population of active galaxies that has come to be known as "Seyfert galaxies," and furthermore such galaxies possess the general nuclear properties of the more luminous QSOs. Large and complete samples of such "classical" Seyfert galaxies will probably be acquired only after extending the apparent-magnitude–limited spectroscopic surveys, such as the CfA redshift survey (Huchra *et al.* 1983), to fainter limiting magnitudes.

TABLE 2

LOG OF OBSERVATIONS

UT Date(s)	Observing Program
1983 Dec 3–5	Spectra of companions
1984 Feb 25–27.....	Long exposures
1984 Jun 27	Photometry (night 13)
1984 Jun 28–29.....	Long exposures
1984 Aug 31.....	Photometry (night 19)
1984 Sep 1	Photometry (night 20)
1984 Oct 23–24.....	Long exposures
1984 Nov 17	Photometry (night 23)
1985 Apr 16.....	Photometry (night 30)

III. OBSERVATIONS AND INITIAL REDUCTIONS

a) Observations

Images of each Seyfert galaxy in the sample were obtained with the University of Hawaii's 2.24 m telescope at Mauna Kea Observatory. A Texas Instruments (TI) 800×800 pixel virtual-phase CCD camera (Hlivak, Henry, and Pilcher 1983) was used at the Cassegrain focus behind a focal reducer, giving a final image scale of $0''.41$ $pixel^{-1}$.

Images were obtained through Kron-Cousins B, V, and R filters of the Kitt Peak "Mould" type. Both a short exposure (typically 60 s) and a long exposure (typically 600 s) were obtained in each filter. A log of the nights on which these observations were made is given in Table 2. Only five nights had both photometric conditions and satisfactory standard star observations. The strategy employed was to obtain at least one "short" exposure of each galaxy in each filter on a photometric night. The long exposures obtained on nights with nonphotometric conditions were subsequently scaled to the photometric observations using the outer regions of the Seyfert galaxies (to avoid the variability of their nuclei and the saturation of the CCD detector in their nuclei). Short exposures also were obtained on nonphotometric nights because (1) they might have better seeing and (2) for conditions to have been considered photometric the sky had to be clear of cirrus clouds both at dusk and at dawn (hence the short-exposure program was carried out on nights that were subsequently determined to have been nonphotometric after examining the sky at sunrise or upon hearing reports of cirrus clouds during the night from observers at other telescopes working in the infrared).

b) Instrumental Corrections

The images were corrected for instrumental effects by the subtraction of an averaged bias frame (obtained from averaging 20–40 0.01 s dark exposures). The usual "extended register" offchip region was used to estimate the DC level of the bias during each exposure to permit scaling of the bias frame prior to its pixel-wise subtraction. Technical problems within the CCD camera's electronics limited the reliability of this estimate of the mean bias level to ~16 electrons rms after correction for day-to-day trends.

Variations in the sensitivity of the CCD from pixel to pixel were corrected with flat-field frames. The flat-field frames were obtained from the average of 2–6 exposures in each filter

of the inside of the dome slit door illuminated with a 75 w photoflood lamp. Each frame was exposed to approximately two-thirds of full well capacity (full well is ~ 70,000 electrons). Flat fields were usually obtained at both the start of the night and also in the morning. These frames were averaged together (except when a large piece of dust appeared on a filter during the night; in those instances, evening flats were used for that part of the night prior to the appearance of the dust particle, and the morning flats were used for the remainder of the night).

The TI virtual-phase CCD detector used for this project has very satisfactory spatial uniformity even prior to the flat-field correction since this frontside illuminated device has not been thinned. At high spatial frequencies the device departs from uniformity by ~ 2% (compared to ~ 8% for the thinned Galileo/Institute for Astronomy TI 500 × 500 three-phase CCD). Furthermore, the only notable features are columns with enhanced sensitivity every 20–25 columns that are satisfactorily corrected with the dome flat-field frames. After division by the averaged flats (containing at least 100,000 electrons pixel^{-1}), the pixel-to-pixel variations are less than 1% (considerably better than the photon statistics in the sky —the deepest exposures have ~ 3000 sky electrons pixel^{-1}). However, larger scale nonuniformities in the device limit the precision to which the area photometry can be conducted (see § III*c*). The TI virtual-phase CCD generates very little, if any, dark current, and the cosmic-ray detection rate over periods of 60–600 s is generally insignificant.

c) *Sky Subtraction*

The images were examined on an image display system and regions surrounding the Seyfert galaxies were extracted for further analysis. These regions ranged in size from ~15% to ~ 75% of the original area of the 800 × 800 pixel CCD detector. The contribution from the night sky was subtracted from these regions by fitting a plane surface of the form (e.g., Watanabe, Koraira, and Okamura 1982):

$$I(x, y) = a_0 + (a_1 x) + (a_2 y),$$

where $I(x, y)$ is the number of counts (1 count = 1.6 electrons) at a point (x, y) within the image. All areas that showed sources (stars, faint galaxies, or the Seyfert galaxy) were excluded from the fit. Values for the shading across the image, defined as

$$(|a_1 x_{\max}| + |a_2 y_{\max}|)/a_0$$

were typically less than 0.02. In general, this procedure removed the sky background to better than 1%. The use of higher order fitting functions did not yield markedly superior results because most of the curvature in the sky background occurs near the edges of the detector (where the optics vignette the field of view). The edges of the detector were not included in most of the regions from which the sky level was determined; in those instances in which the Seyfert galaxy filled most of the frame only a narrow region near the edges was available of the sky level determination (and the simplest fit is desirable in such cases).

d) *Photometric Calibration*

A photometric calibration was obtained for each of the photometric nights by means of observations of standard stars. Both individual stars from the list of Landolt (1983) and, when possible, a selected region in the globular cluster M92 (Christian *et al.* 1985; Heasley 1984) were observed in each filter. Two concentric apertures were centered on each star; the median of the outer aperture was used to determine the local sky level, and the flux in the inner aperture (minus the sky contribution) was measured. Since the second-order color times air mass terms appear to be small (< 0.05 mag air mass^{-1}) and all observations were obtained at less than 1.8 air masses, those terms were set to zero. A least-squares fitting procedure was then used to solve for the relationship:

$$b - B = a_0 + a_1 X + a_2 (B - V),$$

where b is the instrumental magnitude, B is the corrected magnitude, a_0 is the zero point, a_1 is the extinction, a_2 is the color term, and X is the air mass of the observation. Similar forms were used for the V and R passbands.

A mean color term for each filter was determined from the standard star observations obtained on nights 13 and 30 (these being judged the most reliable observations). The standard star observations for each photometric night were then fitted (using these mean color terms), and a zero point and extinction were obtained for each night. Unfortunately, night 19 had too few standard star observations to determine a reliable extinction term; therefore, the extinction from the following night (night 20) was used instead. In an effort to complete the photometry of those Seyfert galaxies visible in the autumn, most of the observations obtained on night 23 were between 1.5 and 1.8 air masses. Regrettably, the high air mass standard star observations on night 23 are unusable because of extremely poor seeing; a fit to the remaining standard stars (with a maximum air mass of 1.4) yields extinction terms several times greater than the typical extinction. Since the standard star observations are somewhat sparse (three Landolt stars each observed 5 times in quick succession) and conditions appeared photometric at both sunset and sunrise, a mean extinction obtained from the average of nights 20 and 30 was used for night 23. It was subsequently found to be necessary to correct the R zero point for night 23 by 0.38 mag in order to force the mean of the $V - R$ colors of the Seyfert galaxies observed on night 23 to agree with the mean of the $V - R$ colors (which have very little scatter) of the Seyfert galaxies observed on the other nights. Since nearly all of the night 23 observations were obtained at similar air masses, this procedure probably results in a final uncertainty of ~ 0.1 mag for night 23, but these observations should be regarded with caution. The remainder of the photometry is probably reliable to 0.05 mag.

IV. ANALYSIS

a) *Profiles*

Profiles of intensity as a function of radius were measured for each galaxy using concentric circular annuli. In the present instance, the most important consideration is the uni-

formity in the treatment of the sample population. Because of the peculiar morphologies of a significant fraction of the galaxies in the sample, ellipse fits to an outer isophote may not provide a reliable indicator of the inclination of the disk components. Therefore the usual practice of fitting a profile obtained from elliptically averaged isophotes was abandoned, and magnitudes were obtained from circular apertures. The position of the nuclear peak was determined from a two-dimensional parabolic fit (with an uncertainty of ~ 0.1 pixels) for the short-exposure images and was estimated from the positions of field stars (with an uncertainty of ~ 1 pixel) for the long-exposure images (which generally have saturated nuclei). The distance from the center of the nucleus was then determined for each pixel in the image, and the counts at that pixel were added into the profile in such a manner that flux is conserved. Regions with field stars or galaxies (except for tightly interacting systems) were excluded from the profile, and each annulus was corrected for the excluded fraction of that annulus.

b) *Point Spread Functions*

The point spread function or "seeing" for each image was determined from measurements of unsaturated stars on each CCD frame. Fits of simple functions to their profiles proved more useful than two-dimensional fits in the subsequent analysis because of the better behavior of the wings of the profiles. When possible, all stars were fitted with both a two-component Lorentzian (Diego 1985) and a two-component gaussian (Thompson 1986). While the Lorentzian usually provided a better fit (especially to the peak of the star images), it failed to converge for stellar images obtained under poor seeing conditions (worse than $\sim 2''$). Neither function fitted trailed images or images contaminated by defective columns on the CCD detector particularly well.

The measured point spread functions (averaging the measured full widths at half-maximum [FWHM] of the B, V, and R images) of the short-exposure images from the photometric nights are listed in Table 1, column (8). Short exposures were obtained for nearly all of the galaxies under nonphotometric conditions on nights with much better seeing than prevailed on nights 23 and 30. While not required for the analysis of the exponential disk parameters, the images with better seeing were used for the morphological classifications and Figures 2–5 (Plates 73–83).

c) *Ellipse Fitting*

To estimate the inclination of each galaxy to our line of sight, an ellipse centered on each galaxy's nucleus was fitted to the 24th magnitude arcsec^{-2} isophote. Because of the superior signal-to-noise ratio resulting from the combination of the generally red colors of the outer parts of the galaxies and the peak in the quantum efficiency of the CCD detector at wavelengths in the R passband, the ellipse fits were performed on the long-exposure R images. Since these images were generally not obtained under photometric conditions, their profiles were scaled to the short, calibrated R profiles over regions external to the nucleus (since the nuclei in the long exposures are usually saturated and since Seyfert nuclei are frequently variable). The ellipses were fitted to the long-exposure R images after smoothing the images twice with a 3×3 kernel. An ellipse centered on the nucleus was fitted to all pixels in the image at the 24th magnitude R isophate (plus or minus a factor sufficient to yield a total of 100–200 pixels for use in the fit—typically < 0.1 mag), all points lying significantly off the fit were discarded, and the fit was repeated. The position angles ("PA"), major axis lengths ("a"), and the ratio of the minor to major axis ("b/a") of each fit are reported in Table 1, columns (12)–(14). The lengths of the axes were determined to ~ 1 pixel (0.″41), and the position angles to $\sim 4°$. For nearly face-on galaxies ($b/a > 0.9$), the position angles become progressively less well determined and become meaningless for $b/a = 1.0$.

d) *Exponential Disk Fits*

Freeman (1970) popularized an exponential model for the light distribution of the outer parts of spiral galaxies of the form:

$$I(r) = I_{(r=0)}e^{-r/r_0},$$

where I is the surface brightness at a radius r and r_0 is the scale length. This function has the convenient properties that a fit to a radial profile expressed in magnitudes is linear and that the central surface brightness is independent of the distance to the galaxy. Its principal unfortunate property is that an exponential will fit almost any profile, and therefore the results are dependent on the correct choice of region in the profile to assign to the disk. In galaxies without active nuclei, the practice has been to fit simultaneously both the disk and the bulge components (using the de Vaucoleurs $r^{1/4}$ law for the bulge). See, for example, the work of Burstein (1979a, b) and Boroson (1981). Kormendy (1977) discusses some potential difficulties with this approach and some limits to the validity of the exponential disk model.

An important factor for the reliable determination of the disk component parameters is the selection of regions in the profiles that are free of contamination by the nucleus or bulge components. The regions selected were linear in surface brightness (expressed in magnitudes) versus radius plots and were extended until the profiles became noisy because of lack of signal. Elliptical isophotes with a single, fixed position angle and ellipticity were used to construct a profile from each smoothed long R passband exposure in a manner similar to that employed in § IVa. For those galaxies with b/a greater than 0.8, circularly averaged profiles were used. (For b/a greater than 0.5, the exponential disk scale lengths obtained from elliptically averaged profiles are larger by a factor of $\sim [2+(a/b)]/3$ than those obtained from circularly averaged profiles.)

The central surface brightnesses were then determined using the scale lengths obtained from the long-exposure R images and from fits to the selected regions in the photometric (short-exposure) profiles. The limiting factors are the choice of regions to fit and the precision of the sky subtraction. Larger galaxies are more likely to have greater sky residuals because they cover a larger region on the CCD detector and also may not provide adequate regions near the edges of the image for determination of the sky. For a few of the smaller

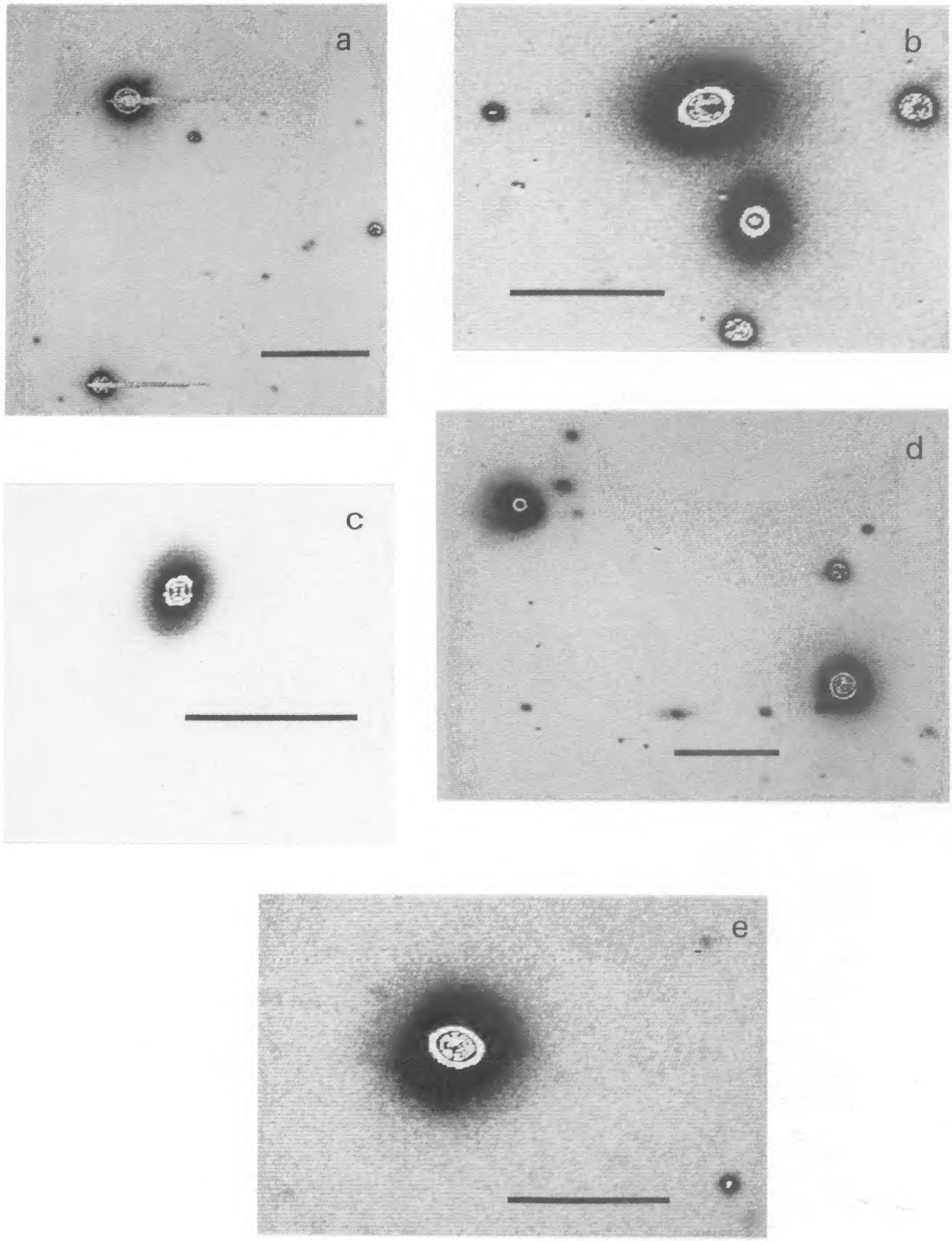

FIG. 2.—Amorphous and unresolved galaxies (MC = 0). In Figs. 2–5 the scale of each image is indicated by a horizontal bar 30″ in length (except where indicated). In all images north is at the top and east is on the left. In most images bright stars and the Seyfert nuclei "wrap around" in the image display, producing a confused white and black region. Often the brightest stars and Seyfert nuclei have saturated the CCD resulting in charge bleeding (to the west). For each image the exposure time and filter is indicated. (*a*) 0004+200 (Mrk 335), 600 s, *R*; (*b*) 0239+070 (Mrk 595), 600 s, *R*; (*c*) 0247+191 (Mrk 372), 600 s, *V*; (*d*) 0323−062 (Mrk 609), 600 s, *V*; (*e*) 0804+391 (Mrk 622), 300 s, *R* (poor seeing).

PLATE 74

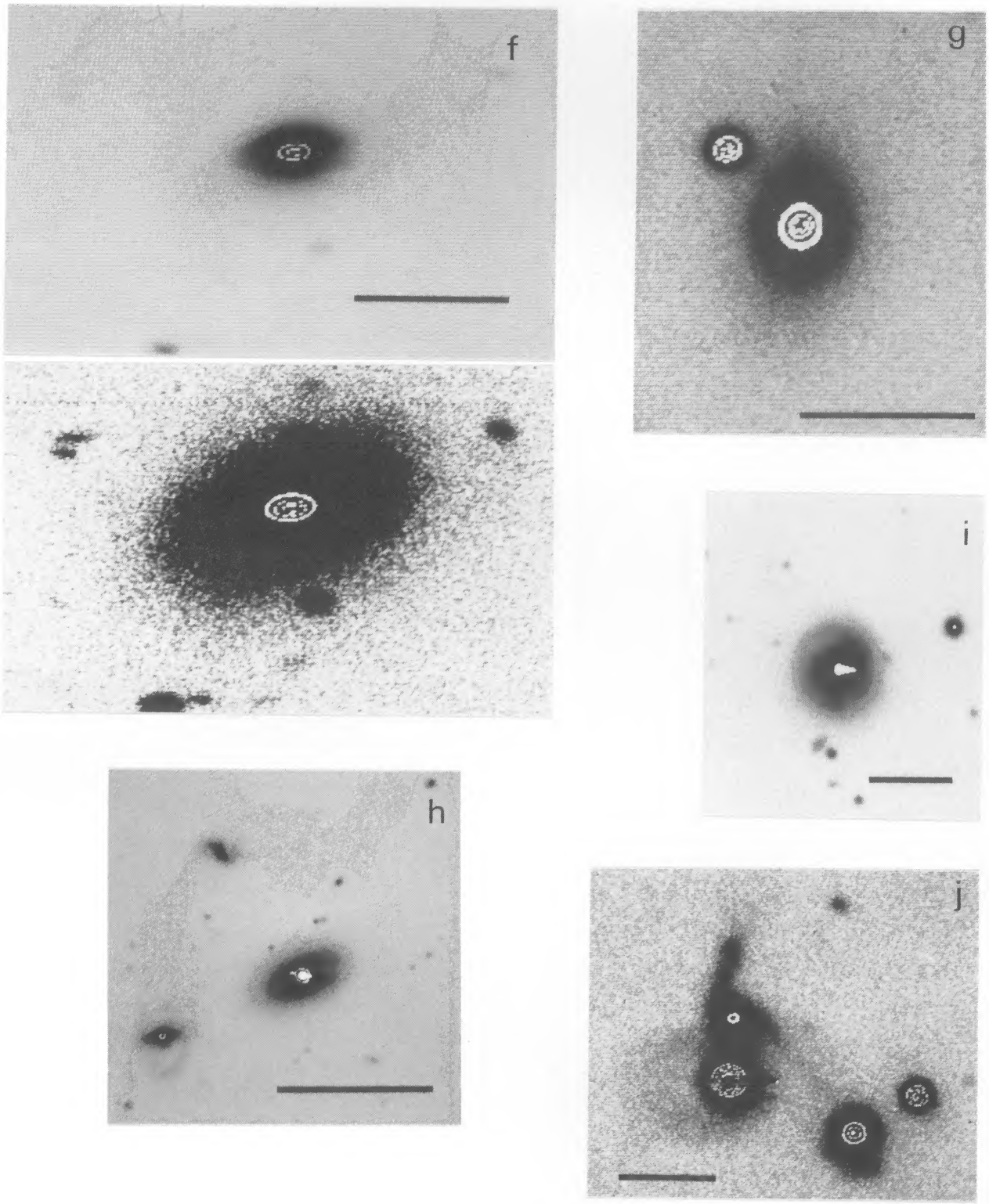

FIGS. 2*f*–2*j*.—Amorphous and unresolved galaxies (MC = 0) continued. (*f*) 1202+204 (NGC 4074), 400 s, *R* (poor seeing); (*g*) 1221+030 (Mrk 50), 600 s, *R*; (*h*) 1339+304 (Mrk 268), 600 s, *R* (scale mark = 60″); (*i*) 1435+590 (Mrk 817), 600 s, *R*; (*j*) 1439+534 (Mrk 477), 600 s, *B*.

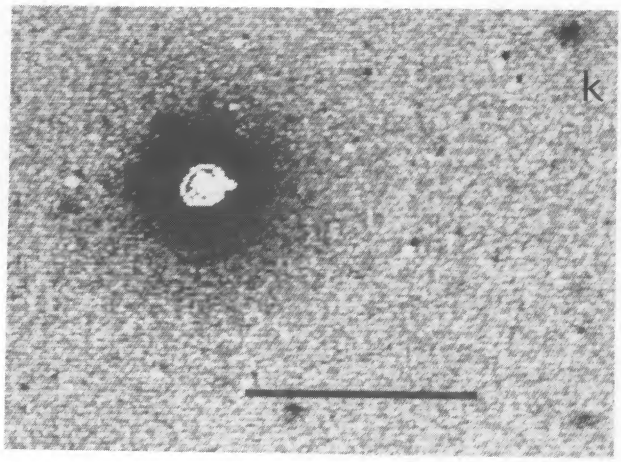

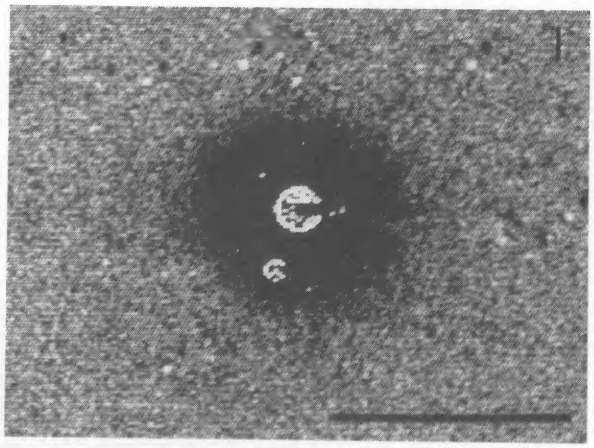

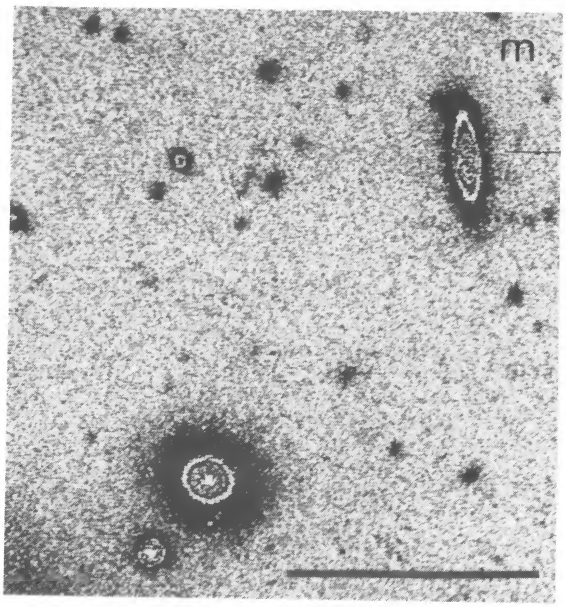

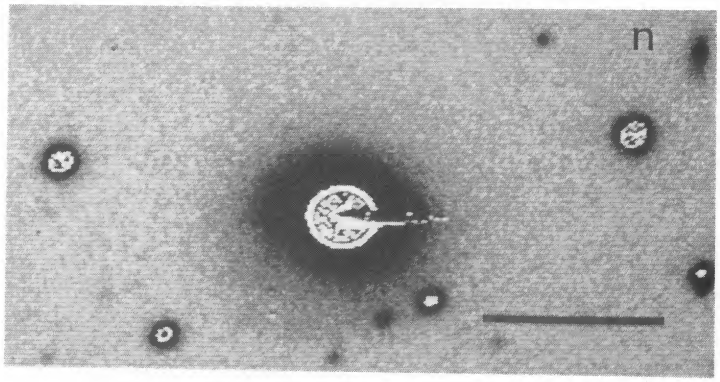

FIGS. 2*k*–2*n*.—Amorphous and unresolved galaxies (MC = 0) continued. (*k*) 1502+104 (Mrk 841), 480 s, *V*; (*l*) 1535+580 (Mrk 290), 480 s, *R*; (*m*) 1622+411 (Mrk 699), 480 s, *R* (scale mark = 60″); (*n*) 2041−105 (Mrk 509), 600 s, *V*.

MACKENTY (*see* **72**, 237)

PLATE 76

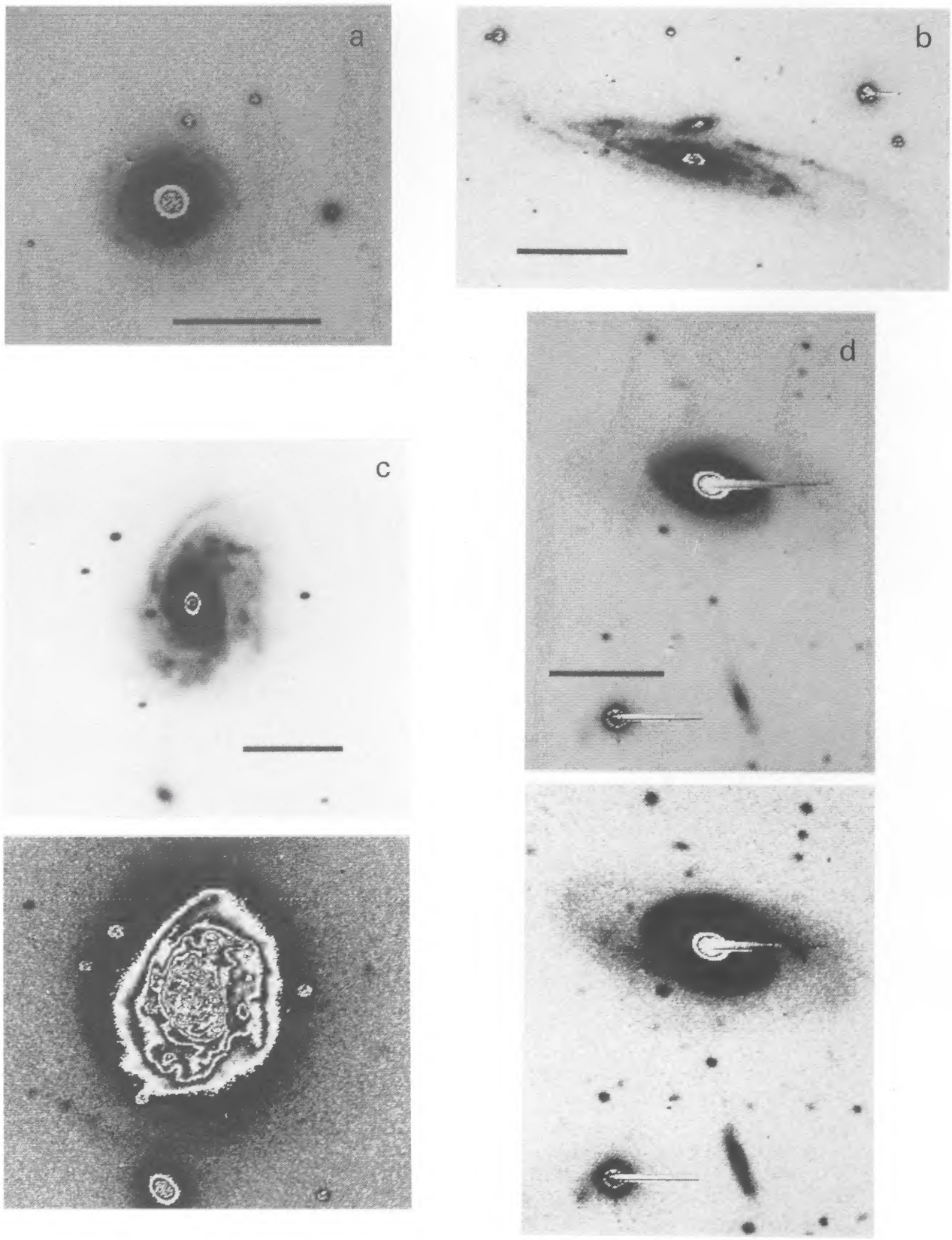

FIG. 3.—Spiral galaxies (MC = 1). (*a*) 0212−010 (Mrk 590, NGC 863), 600 s, *V*; (*b*) 0225+311 (Mrk 1040, NGC 931), 600 s, *B* (scale mark = 60″), (*c*) 0446−062 (NGC 1667), 600 s, *V*; (*d*) 0916+163 (Mrk 704), 1200 s, *R*.

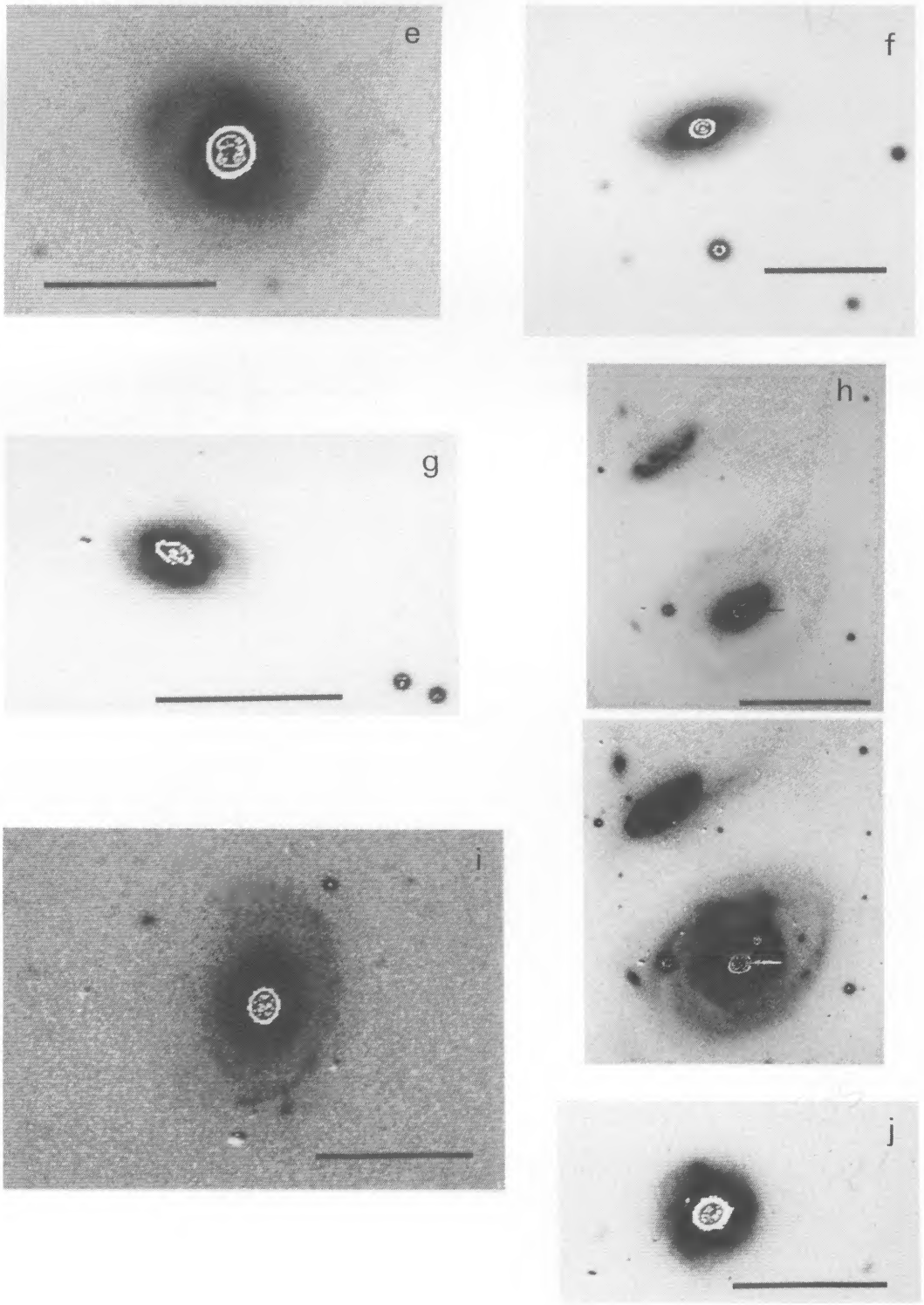

FIGS. 3*e*–3*j*.—Spiral galaxies (MC = 1) continued. (*e*) 1207+472 (Mrk 198), 600 s, *R*; (*f*) 1606+123 (Mrk 871), 600 s, *V*; (*g*) 2154+071 (Mrk 516), 600 s, *V*; (*h*) 2301+084 (NGC 7469), 600 s, *V* (scale mark = 60″); (*i*) 2353+071 (Mrk 541), 600 s, *V*; (*j*) 2359+030 (Mrk 543, NGC 7811), 720 s, *V*.

MACKENTY (*see* **72**, 237)

PLATE 78

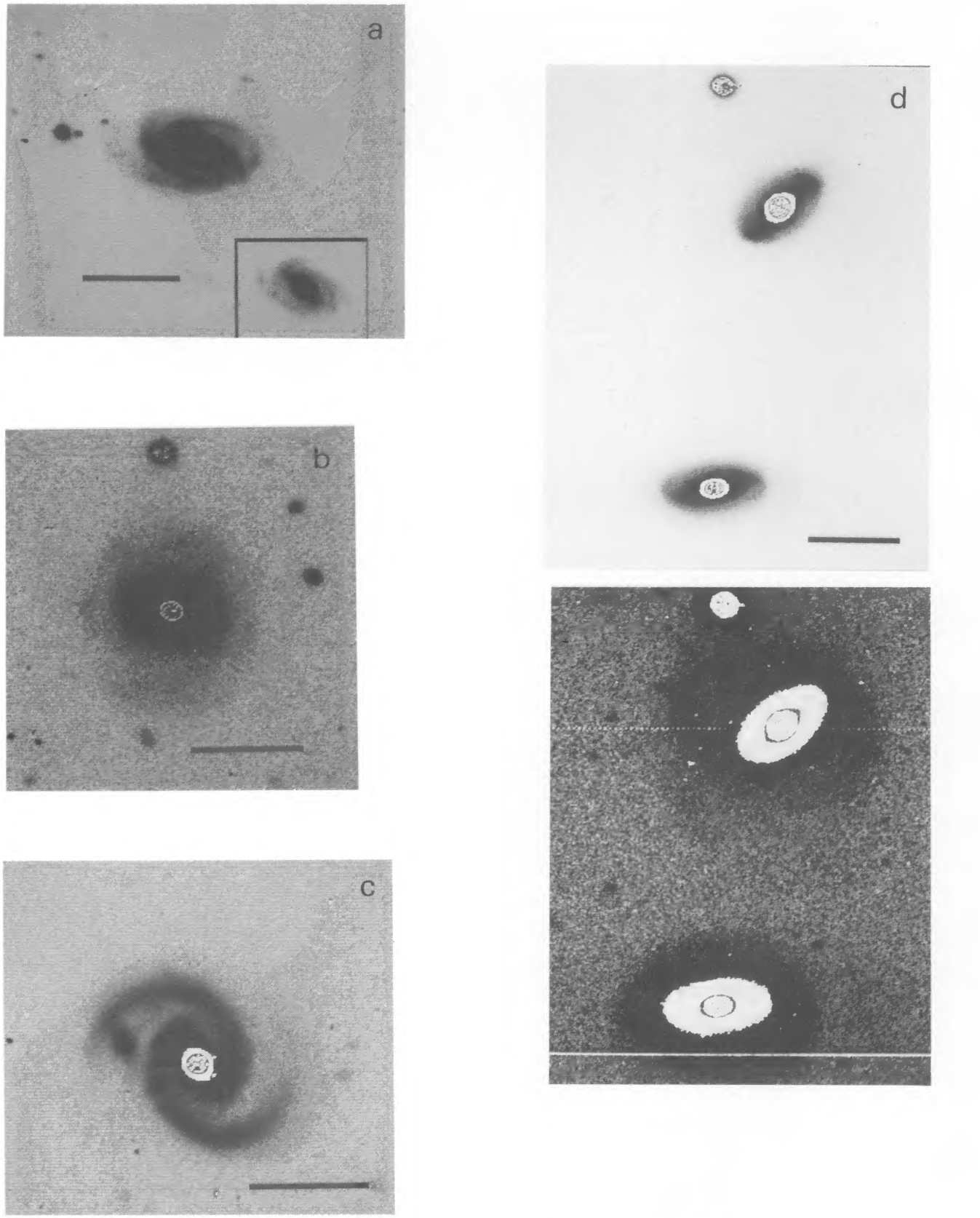

FIG. 4.—Spiral galaxies with bars or rings (MC = 2). (*a*) 0045+143 (Mrk 1146), 600 s, *R*; (*b*) 0228−091 (Mrk 1044), 600 s, *V*; (*c*) 0236+014 (NGC 1019), 600 s, *V*; (*d*) 0328−032 (Mrk 612), 600 s, *V*.

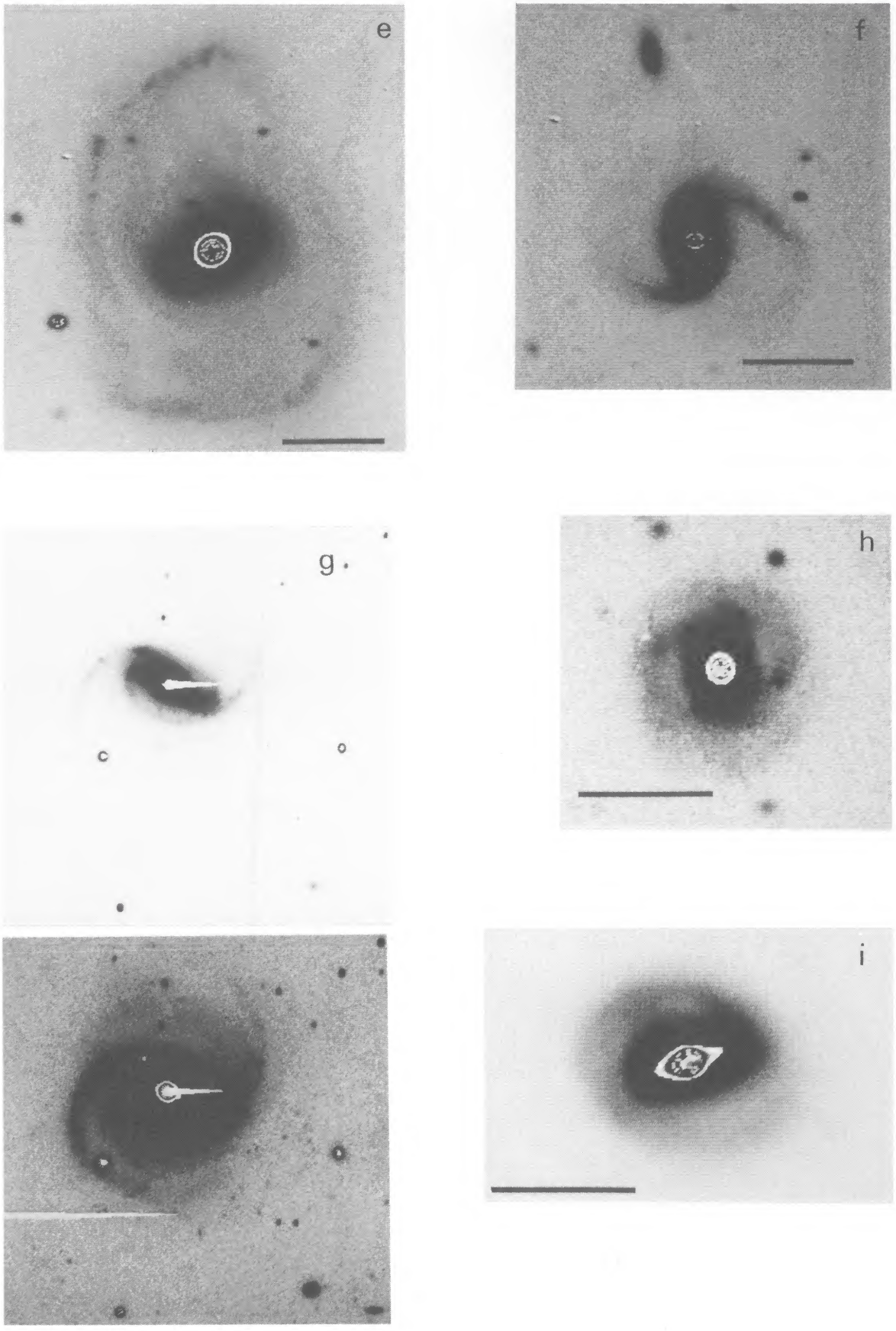

FIGS. 4*e*–4*i*.—Spiral galaxies with bars or rings (MC = 2) continued. (*e*) 0331−052 (NGC 1358), 600 s, *V*; (*f*) 0434−103 (Mrk 618), 600 s, *R*; (*g*) 0739+500 (Mrk 79), 1200 s, *V* (scale uncertain); (*h*) 0752+392 (Mrk 382), 600 s, *R*; (*i*) 1216+301 (Mrk 766, NGC 4253), 600 s, *V*.

PLATE 80

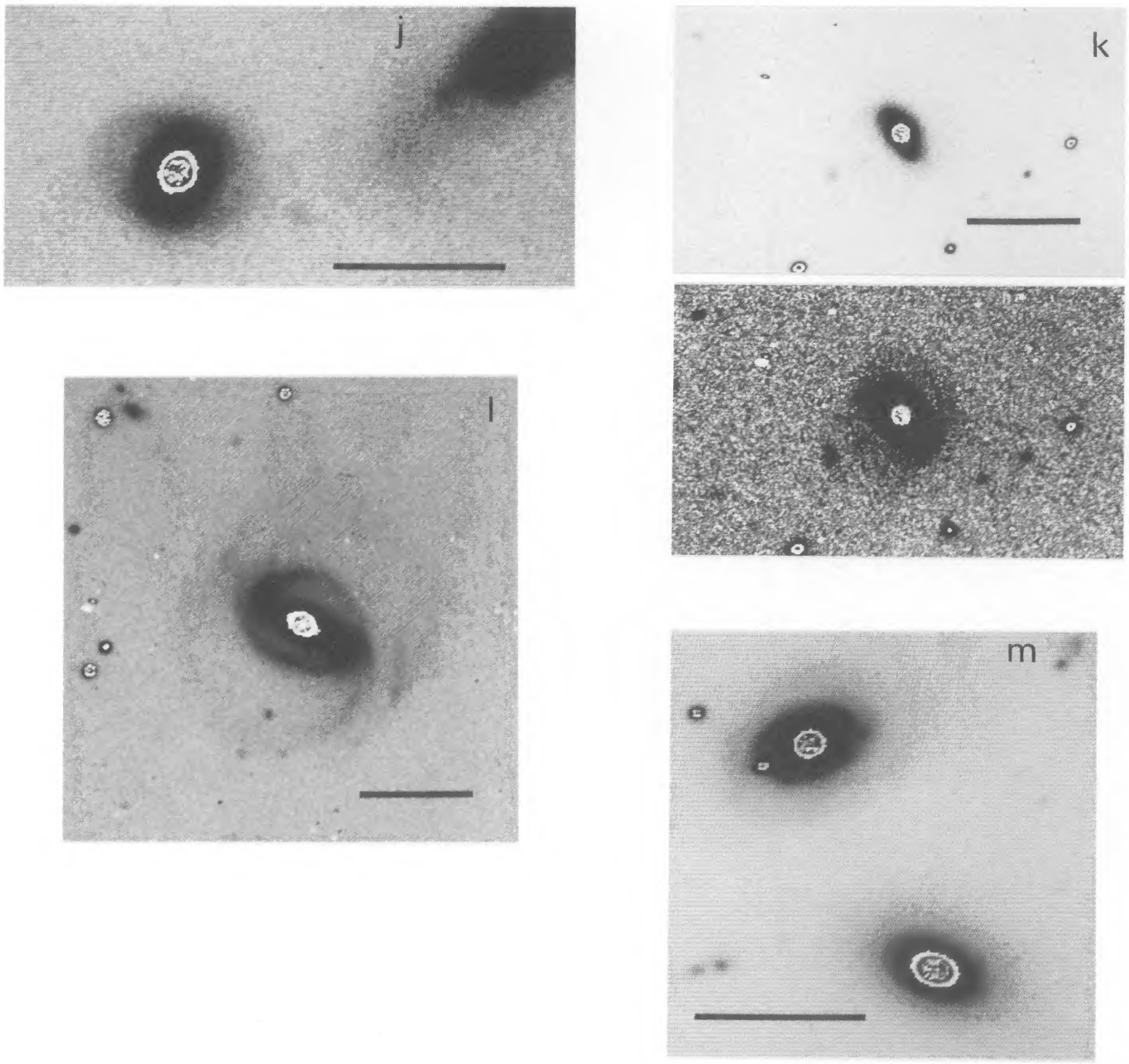

FIGS. 4*j*–4*m*.—Spiral galaxies with bars or rings (MC = 2) continued. (*j*) 1433+485 (Mrk 474, NGC 5683), 600 s, *V*; (*k*) 1553+192 (Mrk 291), 480 s, *V*; (*l*) 1557+351 (Mrk 493), 600 s, *V*; (*m*) 1721+310 (Mrk 506), 900 s, *V*.

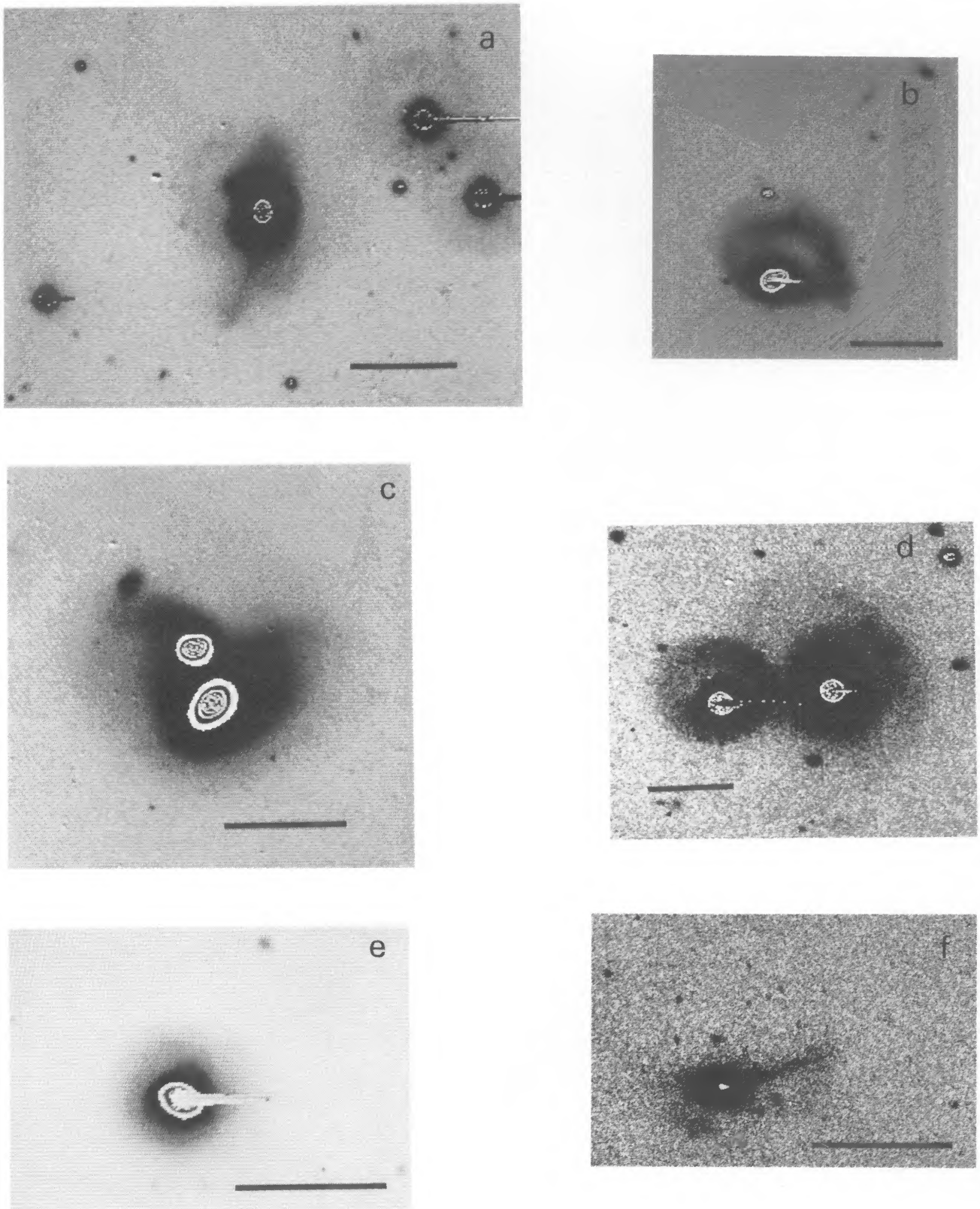

FIG. 5.—Peculiar and interacting galaxies (MC = 3). (*a*) 0204−003 (Mrk 1018), 600 s, *V*; (*b*) 0232−090 (Mrk 1048, NGC 985), 600 s, *R*; (*c*) 0339−013 (NGC 1409), 600 s, *R*; (*d*) 0514−001 (Mrk 1095), 400 s, *V*; (*e*) 0733+585 (Mrk 9), 1200 s, *R*; (*f*) 0922+523 (Mrk 110), 900 s, *R* (scale mark = 60″).

PLATE 82

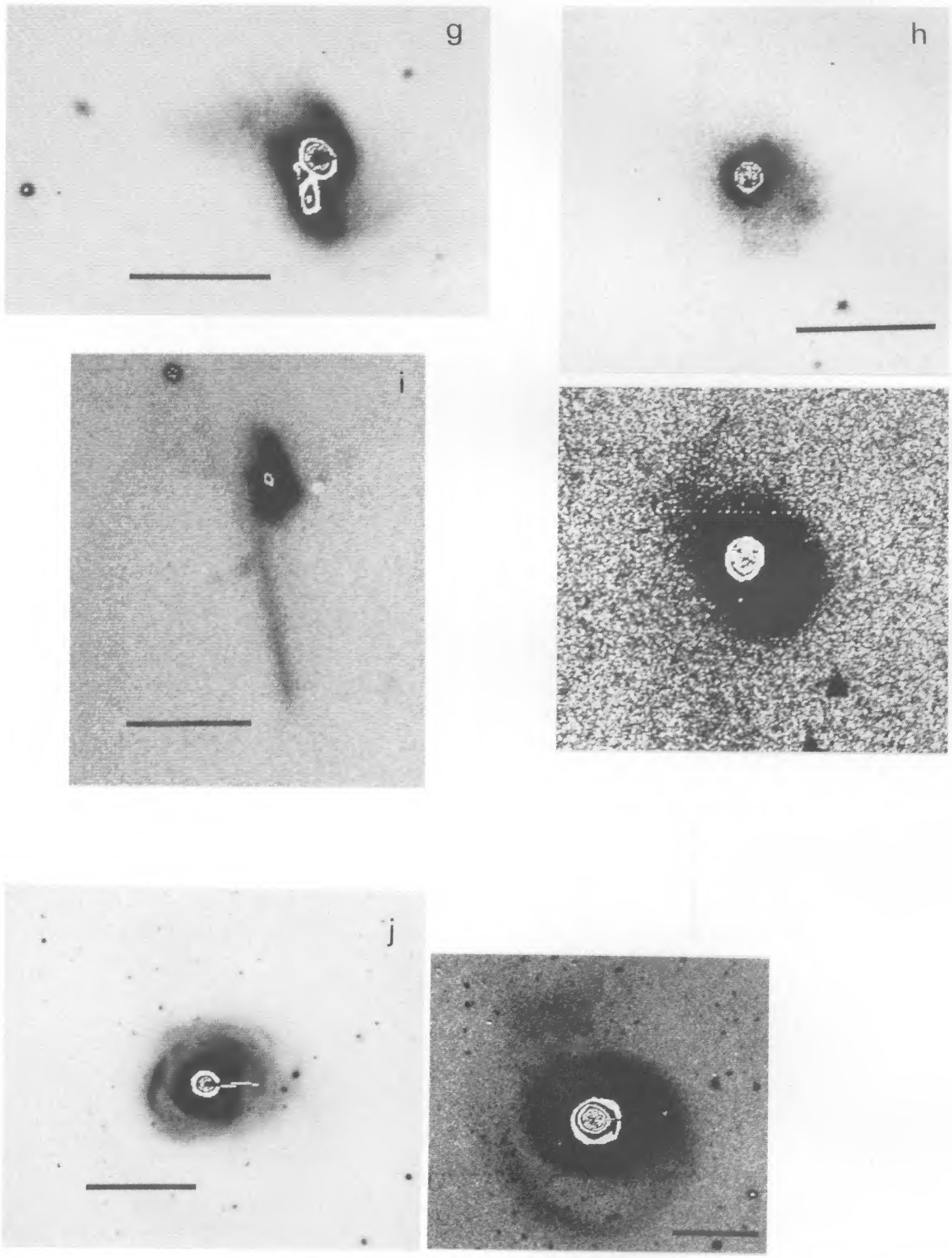

FIGS. 5*g*–5*j*.—Peculiar and interacting galaxies (MC = 3) continued. (*g*) 1124+353 (Mrk 423), 600 s, *R*; (*h*) 1254+571 (Mrk 231), 600 s, *B*; (*i*) 1343+561 (Mrk 273), 600 s, *V*; (*j*) 1416+252 (NGC 5548), 600 s, *R* (scale mark = 60″; the images are at slightly different scales).

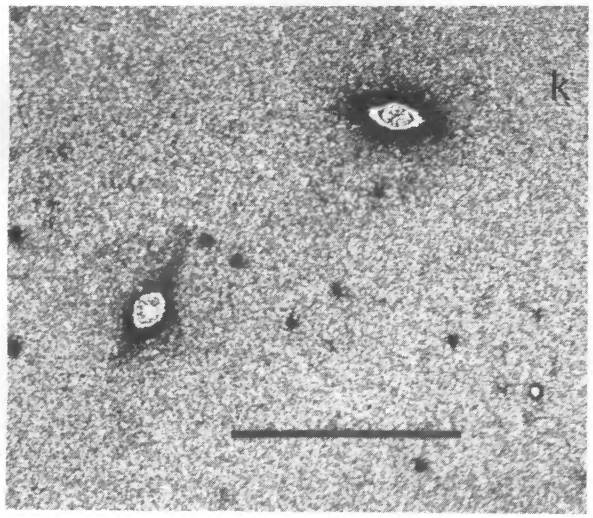

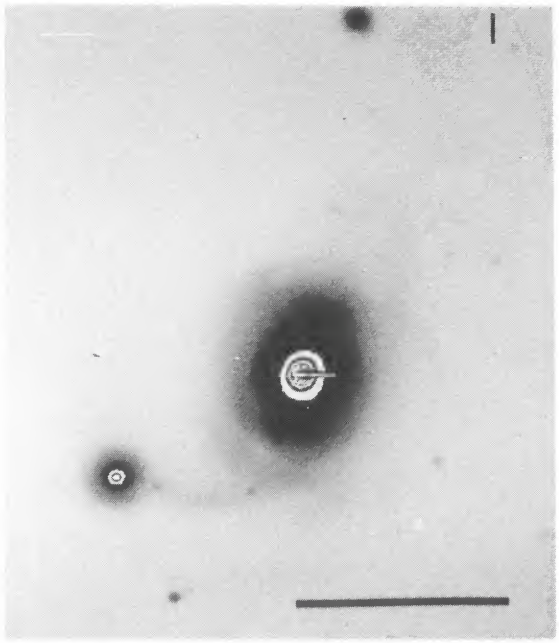

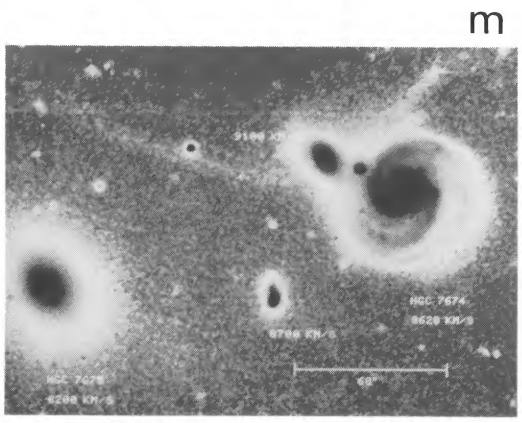

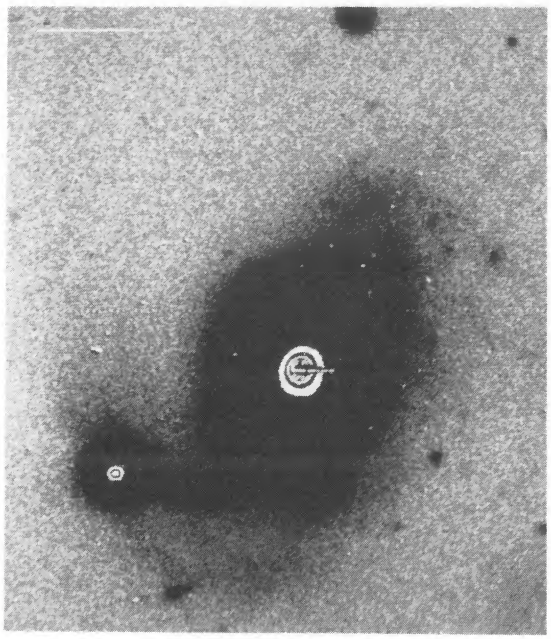

FIGS. 5*k*–5*m*.—Peculiar and interacting galaxies (MC = 3) continued. (*k*) 1535+544 (Mrk 486), 480 s, *V* (scale mark = 60″), (*l*) 2316−000 (Mrk 530, NGC 7603), 1200 s, *V* (scale mark = 60″); (*m*) 2325+083 (Mrk 533, NGC 7674), 700 s (5700–6200 Å passband filter with TI three-phase 500×500 CCD; scale mark indicates 60").

MACKENTY (*see* **72**, 237)

galaxies the disk component is barely evident in the profiles, and the fit may be corrupted by the inclusion of the bulge component. The latter effect will tend to increase the reported central surface brightness. A few cases failed to yield acceptable fits; these are indicated in Table 1, column (15).

V. MORPHOLOGIES

a) Classification Sequences

Several previous surveys of the morphologies of Seyfert galaxies (Adams 1977; Wehinger and Wyckoff 1977; Simkin, Su, and Schwarz 1980; Dahari 1984) demonstrated that Seyfert nuclei are nearly always found in spiral galaxies. The fraction of Seyfert galaxies with peculiar morphologies also appears to be higher than in "normal" galaxies. Since Seyfert galaxies are relatively rare, most are fairly distant and require the best available observational methods. Adams (1977) exploited the image tube, Wehinger and Wyckoff (1977) used an electronographic camera, and Simkin, Su, and Schwarz (1980) restricted themselves to a limited sample (30 galaxies closer than 5000 km s^{-1} in redshift). The present study has been motivated in part by the developement of new detector technology.

The CCD images are presented in Figures 2–5. For each image the filter used and the exposure time are noted in the figure legends. Images have generally been cleaned of visible defects (specifically blocked columns in the CCD detector), and their contrast has been adjusted interactively to yield the "best" representation. The defect that gives rise to a bright spot next to a complementary dark spot is due to dust on the filter. The halos seen around very bright star images are due to reflections in the optical path. In a number of cases (especially galaxies with small bars and galaxies with faint outer features) it has been necessary to present two images of a single galaxy.

Adams (1977) has discussed at some length the difficulties associated with classifying Seyfert galaxies within traditional morphological classification schemes. The principal difficulties are the contribution of the nuclei to the central regions of the galaxies and the greater distance of most Seyfert galaxies compared to galaxies in the existing catalogs of morphological classifications. To demonstrate the limitation in resolution for each of the classifications presented in this study, the size of a resolution element (the FWHM of stars in the image) expressed in kiloparsecs is tabulated in Table 1, column (9). The seeing disk estimates were obtained from the average of the short photometric exposures. Nearly all of the morphological classifications were based on additional images obtained during nights with seeing conditions better than 2".0 and usually better than 1".5.

Each galaxy in the sample has been classified along two sequences, one for morphologies and a second for interactions. Both provide some indication of the likelihood of the presence of mechanisms capable of transporting material into the inner parts of the galaxy. The two sequences are shown in Table 3. The classifications for each galaxy are indicated in Table 1, columns (10) and (11).

TABLE 3

CLASSIFICATION SEQUENCES

Class	Morphology (MC)	Interaction (IC)
0.....	Amorphous/unresolved	Isolated
1.....	Spiral	Companion
2.....	Bar and/or ring	Disturbed companion or at same z
3.....	Peculiar or distorted	Bridge, tail, or jet

NOTES.—Seyfert galaxies with companions with unknown redshifts are classified as IC = 1 if they are approximately the same size as the Seyfert galaxy and are within ~ 5 diameters, or are smaller but within 1 diameter of the Seyfert galaxy.

b) Notes on Individual Galaxies

Redshifts of possible companion galaxies were obtained for several galaxies by the author during the nights of 1983 December 4–5 UT. A grism spectrograph and the TI 500 × 500 three-phase CCD were employed, yielding redshifts accurate only to ~ 200–300 km s^{-1}. Redshifts obtained from these observations have the reference "JWM" and are presented here for the first time.

0004+200 (Mrk 335).—This galaxy is one of a class of barely resolved galaxies dominated by its nucleus. The feature extending several arc seconds toward the NW is intriguing (and within the burned-out region in the image presented by Balick and Heckman 1981, 1982*b*), but since it is not visible in narrow-band [O III] images, it is most likely a background galaxy seen edge-on.

0204−003 (Mrk 1018).—Highly peculiar with a short stubby tail to the SSE. There is an outer "arc" of material to the NE. This galaxy is likely to be a merger.

0212−010 (Mrk 590, NGC 863).—Tightly wound spiral with filamentary arms. There is a small galaxy to the west of unknown redshift.

0225+311 (Mrk 1040, NGC 931).—This well-known galaxy has a small companion that appears distorted. Ward and Wilson (1978) report a velocity difference of 160 km s^{-1}.

0232−090 (Mrk 1048, NGC 985).—This highly peculiar galaxy has a barlike extension to the south and a distorted ringlike feature to the east. Several bright condensations appear in the ring. This galaxy has been discussed by de Vaucouleurs and de Vaucouleurs (1975) and Theys and Spiegel (1976).

0236+014 (NGC 1019).—An unremarkable barred spiral with slightly asymmetric arms except for the small galaxy to the east. A moderate-quality grism spectrum of this galaxy shows emission lines with a redshift within 200 km s^{-1} of the redshift of the Seydfert (JWM).

0239+070 (Mrk 595).—The Seyfert is the larger galaxy to the north. The apparent companion actually is a background galaxy with a redshift greater by 3200 km s^{-1} (Dahari 1985; JWM).

0323−062 (Mrk 609).—The Seyfert is the amorphous galaxy to the SW, and the companion (Mrk 610) is the disturbed galaxy to the NE. Adams (1977) has the identifications re-

versed (see Markkarian and Lipovetskii 1974; Mirabel and Wilson 1984).

0328−032 (Mrk 612).—The Seyfert is the northern barred spiral galaxy. It has faint distorted and fragmented outer arms. The companion barred spiral to the SSE has a redshift difference of 130 km s^{-1} (Dahari 1985; JWM).

0339−013 (NGC 1409, NGC 1410).—A highly distorted interacting pair better known as III Zw 55. There has been some confusion as to which nucleus is the Seyfert (see Wilson and Meurs 1982). Dahari (1985) finds a velocity difference of 480 km s^{-1}, although the distorted appearance convincingly demonstrates the physical association.

0434−103 (Mrk 618).—The small spiral companion to the NNE has an emission-line redshift within 200 km s^{-1} of the Seyfert galaxy (JWM).

0446−062 (NGC 1667).—This spiral galaxy appears to have an anomalous arm along its southern edge opposite a small amorphous galaxy whose redshift is unknown.

0514−001 (Mrk 1095, Akn 120).—The image is complicated by the presence of a nearby bright star. The galaxy is nearly stellar with an extension to the WNW and a faint wisp extending to the NE. The slightly brighter star to the east has a "halo" due to reflections in the focal reducer's optics. A similar halo should be present (but somewhat fainter) around the Seyfert galaxy; the extended material clearly extends well beyond this halo. An [O III] narrow-band image shows an armlike feature extended to the SE.

0733+585 (Mrk 9).—This galaxy appears to be disturbed and shows signs of having spiral arms.

0739+500 (Mrk 79).—This barred spiral galaxy may have an anomalous arm beginning at the nucelus (rather than the end of the bar) and extending to the NE and then around to the SE. The galaxy is also asymmetric, with the northern side of the bar being more diffuse (see Wehinger and Wyckoff 1977).

0804+391 (Mrk 622).—This amorphous galaxy might be a spiral. There is a spiral galaxy of unknown redshift $\sim 3'$ to the WNW.

0922+523 (Mrk 110).—This highly peculiar galaxy has a jetlike tail extending to the WNW. There is a diffuse region at the end of the tail extending to the south. There is also a second extension to the SSE, again possessing a diffuse region at the end. The stellar object embedded in the disturbed body of the galaxy is a foreground star (Adams 1977; Wehinger and Wyckoff 1977; Dahari 1985; JWM). The spectrum of this star obtained as a part of this study adds the Hα line in absorption at zero redshift to the accumulated evidence.

1124+353 (Mrk 423).—Dahari (1985) finds that the interacting companion has a NELG spectrum with a redshift difference of 130 km s^{-1}.

1202+204 (NGC 4074).—This featureless galaxy exhibits a small degree of isophote twisting and a dust lane south of the nucleus extending in an east-west direction.

1207+472 (Mrk 198).—This galaxy may be asymmetric with a brighter arm to the NE.

1216+301 (Mrk 766, NGC 4253).—This barred spiral appears to have an asymmetric arm on its northern side and a ring at the ends of the bar.

1221+030 (Mrk 50).—This amorphous galaxy has a faint plume extending to the north.

1254+571 (Mrk 231).—This peculiar galaxy has a "lumpy" appearance to the SW and a tail to the NNE. There is also a diffuse extended region to the SSE. This galaxy is known for its high-infrared luminosity (Rieke and Low 1975), and its unusual morphology has been recently noted by Hutchings and Neff (1986).

1339+304 (Mrk 268).—This galaxy is possibly a spiral but defies easy classification. The companion to the east has a redshift difference of -890 km s^{-1} (Dahari 1985).

1343+561 (Mrk 273).—This galaxy is perhaps the most peculiar galaxy in the sample. The extension to the south appears to come to an abrupt end and does not point back to the nucleus. The body of the galaxy itself is significantly distored as well. The small segment pointing toward the SE approximately one-third of the way along the extension appears to be associated with the galaxy. There is also faint diffuse material extending to the NE. This galaxy is one of the most luminous galaxies in the *IRAS* catalog (see Fairclough 1986).

1416+252 (NGC 5548).—This well-studied Seyfert galaxy (see e.g., Wilson and Ulvestad 1982) has a distorted inner arm system and a faint outer arm that ends in a diffuse region to the NNE.

1439+534 (Mrk 477, 1 Zw 92).—This system is a good example of a tidal interaction with a bridge connecting the Seyfert (the southwestern galaxy) to its companion. The companion has a bright tail extending to the north and a redshift difference of 220 km s^{-1} (Dahari 1985).

1535+544 (Mrk 486).—This galaxy has a jetlike extension to the NNW with a sickle-shaped plume to the east originating approximately at the end of the extension. Except for the plume, this galaxy might be classified as an edge-on spiral. The companion (I Zw 121-2; Adams 1977) is probably a spiral galaxy. The redshift of the companion is unknown.

1721+310 (Mrk 506).—This galaxy has a prominent ring with faint outer arms. The elliptical galaxy to the SW has a redshift difference of 600 km s^{-1} (Adams 1977).

2041−105 (Mrk 509).—This amorphous galaxy has an asymmetric halo to the south.

2301+084 (NGC 7469).—This well-studied Seyfert (e.g., de Robertis and Pooge 1986; Heckman *et al.* 1986) has an irregular companion with a faint tail to the west.

2302+22 (Mrk 315).—The galaxy appears to be an undistinguished spiral in continuum images. However, there is an extraordinary ionized gas jetlike feature extending 60 kpc to the NW and then bending back toward the SE for a total length of ~ 80 kpc (MacKenty 1986). This feature was discovered in the process of obtaining narrow-band (80 Å) images in the [O III] λ5007 line for ~ 25 of the galaxies in the present sample. Mrk 315 was the only galaxy to show such a dramatic feature. While MacKenty (1986) interpreted this feature as a probable remnant of a tidal interaction, this galaxy does not appear peculiar in the broad-band images and will therefore be considered "normal" in the context of the present study. (An image of this galaxy is not included in this paper; see MacKenty 1986 for images of it.)

2316−000 (Mrk 530, NGC 7603).—This highly disturbed spiral galaxy has been discussed by Arp (1971) and more recently by Sharp (1986). The small galaxy to the SE has a redshift 7700 km s^{-1} greater than that of the Seyfert (Arp 1971; Dahari 1985; JWM). In agreement with Sharp (1986), the CCD images obtained here show two arms or tails crossing the "companion" galaxy and extending beyond it. The original assertion by Arp (1971) that the "arm" ended at the "companion" galaxy is not borne out by the deeper images.

2325+083 (Mrk 533, NGC 7674).—This galaxy is probably the best example of a "classical" Toomre-type (Toomre and Toomre 1972) interaction in this sample. The Seyfert is the spiral galaxy to the west in this small group. It displays two long "tidal tails," one extending to the ENE and the other extending to the NW. The elliptical to the east has a redshift difference of −270 km s^{-1} (Dahari 1985; JWM), and both of the two smaller galaxies have redshifts within 300 km s^{-1} of the Seyfert galaxy (JWM). The small galaxy to the SE appears to be distorted and has emission lines.

VI. DISCUSSION

a) Morphologies

The most striking result of this survey is the widespread prevalance of disturbed, interacting, or peculiar galaxies. Many of the remaining galaxies have bars or rings. Half of the galaxies in this sample have either a disturbed morphology or a bar. The two-dimensional distribution of the classification sequences is shown in Table 4. If we treat all the amorphous galaxies (27% of the sample) as belonging to a special class (either intrinsically or as the result of the resolution of the available images; see § VI*d*) and exclude them from consideration, then 35% of all "spiral" Seyfert galaxies in the sample are peculiar and 70% have either disturbed morphologies or bars.

The classifications assigned in Table 1, columns (10) and (11), represent fairly conservative assignments. Where the images are suggestive of the presence of spiral arms, a bar or a ring, or a distorted morphology, an alternative classification is given in parentheses. With the alternative classifications, 65% of all galaxies and 79% of all nonamorphous galaxies have either a bar or a disturbed morphology.

The fraction of barred spirals is the same as found in "normal" galaxies. Of the 51 galaxies in this sample, at least 13 and perhaps as many as 17 have bars (25%–33%). In the revised Shapley-Ames catalog (Sandage and Tammann 1981), 26% of all spiral galaxies and 36% of Sa0-Sbc galaxies exhibited bars. The presence of a bar is nonetheless of interest in the context of this paper since bars appear to channel material into the inner regions of galaxies (Heckman 1980*b*, and references therein). Hawarden *et al.* (1986) report that the infrared luminosity of nuclei is enhanced in barred galaxies.

Seyfert galaxies are more likely than non-Seyfert galaxies to be found in peculiar or disturbed systems. Determining the fraction of all galaxies with peculiar or disturbed morphologies is somewhat difficult. Such classifications depend on both the limiting sensitivity of the observations and the resolution; for example, the "shells" found around some elliptical galaxies (e.g., Malin and Carter 1983). Probably only a few percent of all spiral galaxies would be classified as peculiar on the system used in this study. Lonsdale, Persson, and Matthews (1984) used the work of Arp and Madore (1977) to estimate that 3%–6% of all galaxies might be classified as peculiar. When that fraction is compared to the 25%–35% of the galaxies in this sample that exhibit peculiar morphologies, it is evident that the Seyfert galaxies are strikingly unusual.

Only 22% (18% in the alternative classifications) of the galaxies in the sample are undisturbed spirals without bars. Excluding those with companions (IC = 2 or IC = 3) decreases this fraction to 18% (10%). If the few isolated spirals in fact do not have undetected bars or morphological peculiarities, a more careful study of these galaxies is clearly warranted.

TABLE 4

TWO-WAY MORPHOLOGY CLASSIFICATIONS

	IC				
MC	0	1	2	3	Total
0.....	9	2	2	1	14
1.....	6	3	2	0	11
2.....	8	1	3	1	13
3.....	9	1	0	3	13
Total ...	32	7	7	5	51

b) Magnitudes and Colors

Magnitudes and colors derived from the circularly averaged profiles (§ IV*a*) are tabulated in Table 1, columns (16)–(24), for each galaxy for a 30 kpc diameter aperture (encompassing essentially the entire detected galaxy in nearly all cases), for a 5 kpc diameter aperture, and for an annulus covering the region between 5 and 10 kpc in radius from the nuclei (i.e., the annulus has inner and outer diameters of 10 and 20 kpc). The 5 kpc diameter aperture was selected as the smallest achievable without becoming smaller than the seeing disks of the observations with the poorest resolution. The 5–10 kpc annulus was chosen to be outside of the region dominated by the nucleus and the bulge. These apertures will henceforth be referred to as the "nucleus" and "disk" apertures.

Figure 6 shows the distribution of the absolute V magnitudes for the 30 kpc apertures. The peculiar and disturbed galaxies (MC = 3) are generally brighter. In three instances the photometry includes the second nucleus of an interacting system (or a foreground star in the case of Mrk 110). While this would act to increase the total magnitude of the system, these galaxies are among the least luminous of the MC = 3 galaxies.

There is very little variation in the $V - R$ colors of both the nuclei (mean = 0.59, standard deviation = 0.09) and the disks (0.54, 0.10). The $B - V$ colors of the nuclei (0.61, 0.26) and of the disks (0.75, 0.17) show a much greater dispersion. The distribution of $B - V$ colors for the nuclei and the disks is shown in Figure 7. The amorphous (MC = 0) and peculiar (MC = 3) galaxies more often have blue nuclei than either the barred spiral (MC = 2) or the spiral (MC = 1) galaxies.

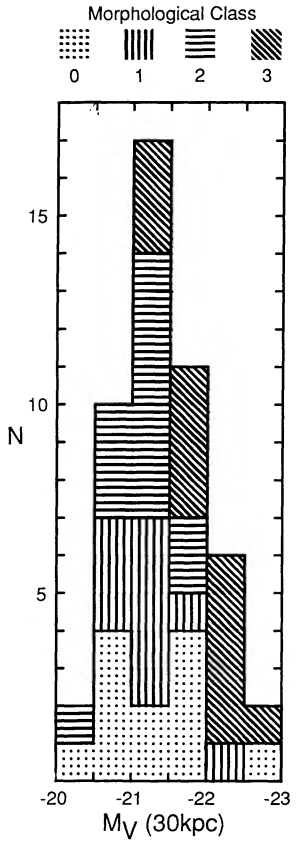

FIG. 6.—The absolute V magnitudes within 30 kpc diameter apertures are shown with each morphological class (MC) as indicated by the key. The peculiar galaxies (MC = 3) tend to be brighter than average. The key at the top of this figure also applies to Figs. 8–10 and 12–13.

c) *Decompositions*

The disk components of spiral galaxies have been studied extensively (Freeman 1970; Burstein 1979*a*, *b*; Boroson 1981) and display some consistent properties (but see Kormendy 1977). Boroson (1981) found that the central surface brightnesses of the disks tend to cluster around 21.8 B mag arcsec^{-2} (this value is independent of distance). The disk scale lengths fall within the range of 1 to 5 kpc (Freeman 1970) and 1 to 10 kpc (Boroson 1981). The results of fitting an exponential disk model to the galaxies in the present sample are reported in Table 1, columns (15) and (25)–(27). Galaxies with $b/a < 0.5$ and galaxies whose profiles lack an identifiable "disk" region are indicated in Table 1, column (15), and are excluded from the following analysis of the disk parameters.

The central surface brightnesses in B, corrected for their inclination and extinction within our Galaxy by

$$B(0)_c = B(0) + 2.5 \log (a/b) - 0.2 \csc |b^{II}|$$

are shown in Figure 8. The mean corrected central surface brightness is 21.9 B mag arcsec^{-2} (with a 1 σ dispersion of 1.0 mag). The correction for the use of circularly averaged profiles was found empirically to be less than 0.2 mag in R for $b/a = 0.6$–0.8. This value for the mean central surface brightness is in good agreement with the values of Freeman (1970) and Boroson (1981). Yee (1983) tentatively concluded that Seyfert galaxies might have somewhat brighter central surface brightnesses than normal spirals (he found an average value of 21.3). That finding is not confirmed by the present results. A comparison of the regions Yee (1983) selected for his disk fits may explain the higher central surface brightnesses he found. The fits reported here seldom include regions of the profiles inside of 10″ and typically begin 15″ or more from the centers of the galaxies. Yee (1983) fit profiles between 5″ and 15″ from the more distant galaxies and between 10″ and 25″ from the closer ones due to the limitations of the SIT detector used in his study. It seems probable that this inadvertently included a sizable contribution from the bulges or nuclei of the galaxies in his fits to the "disk" components.

The fraction of the luminosity in the disk component within a 32 kpc diameter aperture (see Yee 1983) is shown in Figure 9. There is a possible tendency for both the peculiar and the amorphous galaxies to have less dominant disks than the spiral and barred spiral galaxies. As might be expected as a result of the blue colors of the Seyfert nuclei, there is an inverse correlation between the fraction of the luminosity in the disk component and the $B-V$ colors of the nucleus; no correlation is seen with the $B-V$ disk colors.

The disk scale lengths (r_0) are shown in Figure 10. The amorphous galaxies generally have shorter scale lengths than the other galaxies. The lengths of the major axes at the 24th mag arcsec^{-2} isophote of the amorphous galaxies are also generally smaller. There may be a tendency for both the scale lengths and major axis lengths of the peculiar galaxies to be larger than average. Freeman (1970) found that the range of the scale lengths is correlated with morphology. Early-type spiral galaxies have a larger range in scale lengths (up to 7 kpc), while late-type spiral galaxies generally have scale lengths less than ~ 2 kpc. The implication of the observed distribution is that Seyfert galaxies are generally found in early-type spirals.

d) *Amorphous Galaxies*

The class of Seyfert galaxies classified here as "amorphous or unresolved" have drawn only limited attention in the past (e.g., Adams 1977). These galaxies constitute between 18% and 27% of the sample. Several of these galaxies show some kind of feature but are difficult to classify (i.e., Mrk 372 [0247+191], Mrk 622 [0804+391], NGC 4074 [1202+204], Mrk 268 [1339+304], and Mrk 817 [1435+590]). Furthermore the observations of Mrk 609 (0323−062) have relatively poor resolution, and it is therefore difficult to classify (although its companion of the same size has visible structure in the same CCD images). Even without these five galaxies, there are eight amorphous galaxies in the sample whose lack of further classification cannot be explained by poor resolution. Figures 11 and 12 show the distribution of the morphological classes in resolution and in redshift. The presence of the amorphous galaxies is evidently not due to any limitations in the available images. Adams (1977) discussed four of these (Mrk 335 [0004+200], Mrk 50 [1221+030], Mrk 290 [1535+580], and Mrk 509 [2041+105]) and considered them unresolved or

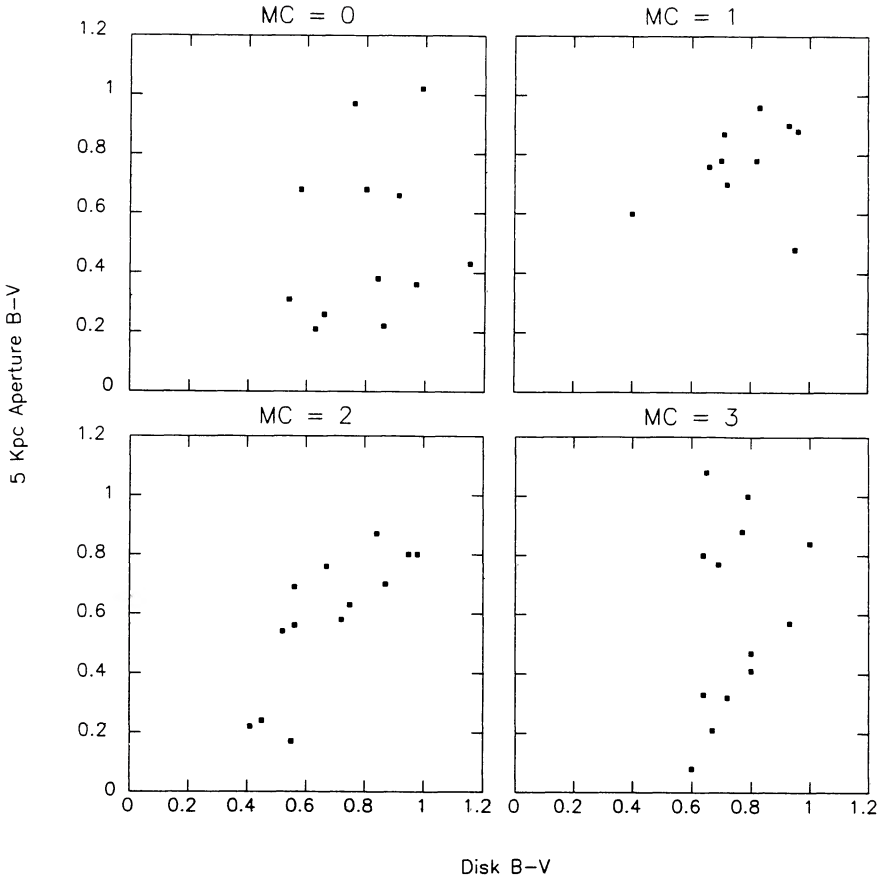

FIG. 7.—The $B-V$ colors within a 5 kpc diameter aperture are shown against the $B-V$ colors within a 5–10 kpc radius annulus for each morphological class.

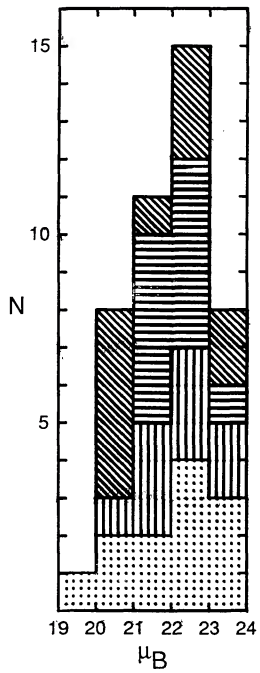

FIG. 8.—The central surface brightness in B obtained from fitting the exponential disk components are shown in magnitudes per square arcsecond. No particular trend with morphological class is evident.

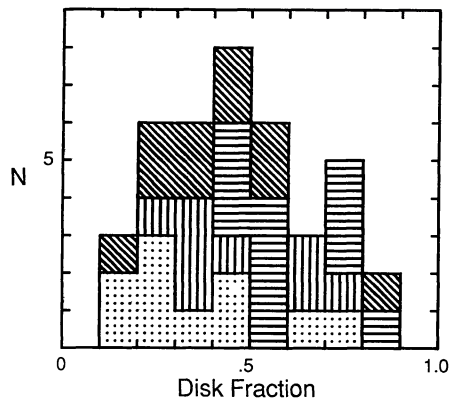

FIG. 9.—The fraction of the luminosity in the exponential disks in the V passband is shown by morphological class. Both amorphous galaxies (MC = 1) and peculiar galaxies (MC = 3) appear to have somewhat less of their total luminosity in their disks.

potential ellipticals. The $B-V$ colors of the "disk" regions of these galaxies are not particularly red compared to the rest of the sample. These galaxies tend to have smaller sizes and shorter exponential disk scale lengths. The distribution of the axial ratios (b/a) at the 24th magnitude R isophote is shown in Figure 13. Although the amorphous galaxies preferentially

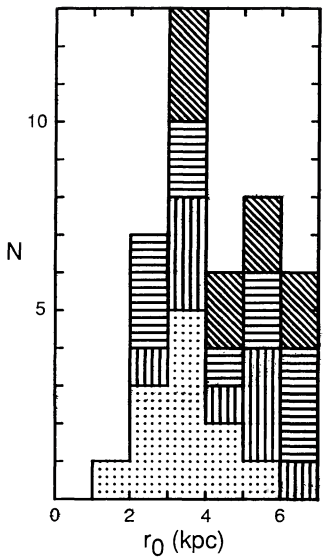

FIG. 10.—The exponential disk scale lengths (in kiloparsec) are shown by morphological class. The amorphous galaxies (MC = 0) generally have shorter scale lengths.

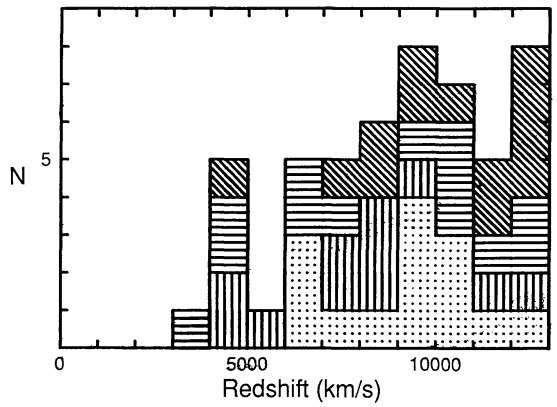

FIG. 12.—The morphological classes are displayed as a function of redshift. This further illustrates the reality of the amorphous class of galaxies.

appear circular or "face-on," they occupy essentially the entire range of observed ratios. Keel's (1980) finding that Seyfert galaxies generally have ratios of greater than 0.5 is confirmed.

In light of both the above and the relative ease with which other Seyfert galaxies at the same resolution were classified, it appears that a majority of the amorphous (MC = 0) galaxies are intrinsically amorphous. Since their colors indicate that these galaxies are unlikely to be elliptical galaxies, a possible interpretation is that these galaxies are the remnants of prior interactions or megers. If this is indeed the case, a study of the stellar population of these galaxies might provide insight into the lifetime of the Seyfert phenomena. To some extent the amorphous galaxies resemble class II irregular galaxies or blue compact galaxies (see Sandage and Brucato 1979; Thuan 1983; Noreau and Kronberg 1986). Sandage and Brucato (1979) report mean $B-V$ colors of ~ 0.6 in accord with the colors of the MC = 0 galaxies. Noreau and Kronberg (1986) discuss an amorphous galaxy in an interacting system. Several

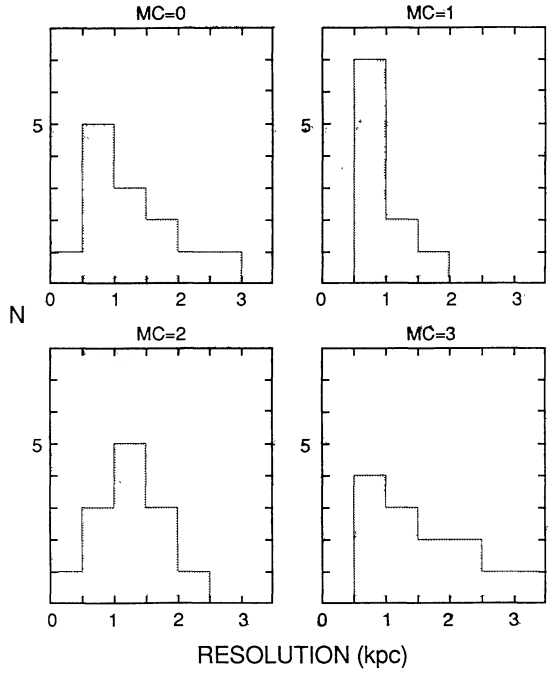

FIG. 11.—The resolution of the short-exposure photometric images is shown for the observations of the galaxies in each morphological class. The resolution is defined here as the size of the seeing disk expressed in kiloparsecs. It is clear that the amorphous classification does not reflect merely inferior imagery.

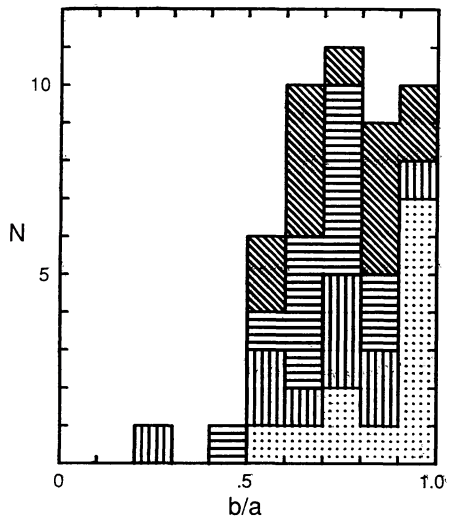

FIG. 13.—The minor to major axis ratios (b/a) are shown as a function of morphology. Although most of the amorphous galaxies are round, a significant tail exists of more elliptically shaped galaxies. The tendency for the barred spirals (MC = 2) to avoid appearing face-on is probably the result of the bar's influence on the ellipse fitting procedure.

authors have recently discussed the possibility of significant star formation in these galaxies (e.g., Gondhalehar *et al.* 1986).

VII. SUMMARY

The results of this study extend the work of Adams (1977), Wehinger and Wyckoff (1977), Simkin, Su, and Schwarz (1980), and Yee (1983) in two major dimensions. First, it appears that Seyfert galaxies without a mechanism for moving material into their nuclei (i.e., a bar or external perturbation) are the exception rather than the rule. Second, the class of Seyfert galaxies with amorphous morphologies appears to represent a significant fraction of all Seyfert galaxies. If the speculation that these galaxies are the result of earlier perturbations or mergers is indeed correct, then an even larger fraction of the Seyfert galaxies have evidence for large-scale disruptions.

I am deeply grateful to my thesis advisor Alan Stockton for his support, encouragement, and guidance. Jim Heasley, Laird Thompson, Gareth Wynn-Williams, and Andrew Wilson made helpful comments on this manuscript. I have had helpful discussions with Oved Dahari, Gary Hill, and Brent Tully. Bob Hlivak, Carl Pilcher, and Pat Henry made the Galileo/IfA CCD camera system a very useful instrument. I am indebted to Carl Pilcher for providing me with his filter wheel assembly. Frank Cheigh and the staff of the UH 88 inch telescope were most helpful. I am grateful to A. Schinckel for providing a computer tape of his unpublished catalog of active galaxies. Louise Good helped with the manuscript preparation. The STScI art department aided in the construction of the figures. Financial support has been provided by the Honolulu Chapter of the Achievement Rewards for College Scientists Foundation and National Science Foundation grants AST 83-17457 and AST 80-22203 to Alan Stockton.

REFERENCES

Adams, T. F. 1977, *Ap. J. Suppl.*, **33**, 19.
Arp, H. 1971, *Ap. Letters*, **7**, 221.
Arp, H. C., and Madore, B. F. 1977, *Quart. J.R.A.S.*, **18**, 234.
Balick, B., and Heckman, T. M. 1981, *Ap. J.*, **247**, 32.
_____. 1982*a*, *Ann. Rev. Astro. Ap.*, **20**, 431.
_____. 1982*b*, *Ap. J.*, **256**, 798.
Balzano, V. A. 1983, *Ap. J.*, **268**, 602.
Boroson, T. 1981, *Ap. J. Suppl.*, **46**, 177.
Boroson, T. A., and Oke, J. B. 1982, *Nature*, **296**, 397.
Boroson, T. A., Persson, S. E., and Oke, J. B. 1985, *Ap. J.*, **293**, 120.
Burstein, D. 1979*a*, *Ap. J. Suppl.*, **41**, 435.
_____. 1979*b*, *Ap. J.*, **234**, 435.
Christian, C. A., Adams, M., Barnes, J. V., Butcher, H., Hayes, D. S., Mould, J. R., and Siegel, M. 1985, *Publ. A.S.P.*, **97**, 363.
Dahari, O. 1984, Ph.D. thesis, University of California, Santa Cruz.
_____. 1985, *Ap. J. Suppl.*, **57**, 643.
de Grijp, M. H. K., Miley, G. K., Jub, J., and de Jong, T. 1985, *Nature*, **314**, 240.
de Robertis, M. 1985, *A.J.*, **90**, 998.
de Robertis, M. M., and Pogge, R. W. 1986, *A.J.*, **91**, 1026.
de Vaucouleurs, G., and de Vaucouleurs, A. 1975, *Ap. J. (Letters)*, **197**, L1.
Diego, F. 1985, *Pub. A.S.P.*, **97**, 1209.
Fairclough, J. H. 1986, *M.N.R.A.S.*, **219**, 1P.
Fosbury, R. A. E., *et al.* 1982, *M.N.R.A.S.*, **201**, 991.
Freeman, K. C. 1970, *Ap. J.*, **160**, 811.
Gaskell, C. M. 1985, *Nature*, **315**, 386.
Gondhalekar, P. M., Morgan, D. H., Dopita, M., and Ellis, R. S. 1986, *M.N.R.A.S.*, **219**, 505.
Gunn, J. E. 1979, in *Active Galactic Nuclei*, ed. C. Hazard and S. Mitton (Cambridge: Cambridge University Press), p. 213.
Hawarden, T. G., Mountain, C. M., Leggett, S. K., and Puxley, P. J. 1986, *M.N.R.A.S.*, **221**, 41P.
Heasley, J. N. 1984, private communication.
Heckman, T. M. 1980*a*, *Astro. Ap.*, **87**, 152.
_____. 1980*b*, *Astr. Ap.*, **88**, 365.
Heckman, T. M., Balick, B., and Sullivan, W. T., III. 1978, *Ap. J.*, **224**, 745.
Heckman, T. M., Beckwith, S., Blizt, L., Skrutskie, M., and Wilson, A. S. 1986, *Ap. J.*, **305**, 157.
Heckman, T. M., Bothun, G. D., Balick, B., and Smith, E. P. 1984, *A.J.*, **89**, 958.
Hewitt, A., and Burbidge, G. 1980, *Ap. J. Suppl.*, **43**, 57.
Hlivak, R. J., Henry, J. P., and Pilcher, C. B. 1984, *Proc. SPIE*, **445**, 122.
Huchra, J., Davis, M., Latham, D., and Tonry, J. 1983, *Ap. J. Suppl.*, **52**, 89.
Huchra, J., and Sargent, W. L. W. 1973, *Ap. J.*, **186**, 433.
Huchra, J. P., Wyatt, W. F., and Davis, M. 1982, *A.J.*, **87**, 1628.
Hutchings, J. B., Crampton, D., and Campbell, B. 1984, *Ap. J.*, **280**, 41.
Hutchings, J. B., Crampton, D., Campbell, B., Gower, A. C., and Morris, S. C. 1982, *Ap. J.*, **262**, 48.
Hutchings, J. B., Crampton, D., Campbell, B., and Pritchet, C. 1981, *Ap. J.*, **247**, 743.
Hutchings, J. B., and Neff, S. G. 1987, in *IAU Symposium 121, Observational Evidences of Activity of Galaxies*, ed. E. Ye. Khachikian, K. J. Fricke, and J. Melnick (Dordrecht: Reidel), p. 399.
Kalloglian, A. T. 1971, *Astrofizika*, **7**, 521.
Keel, W. C. 1980, *A.J.*, **85**, 198.
_____. 1985, *A.J.*, **90**, 1449.
Kormendy, J. 1977, *Ap. J.*, **217**, 406.
Landolt, A. U. 1983, *A.J.*, **88**, 439.
Lawrence, A., and Elvis, M. 1982, *Ap. J.*, **256**, 410.
Lonsdale, C. J., Persson, S. E., and Matthews, K. 1984, *Ap. J.*, **287**, 95.
MacKenty, J. W. 1986, *Ap. J.*, **308**, 571.
MacKenty, J. W., and Stockton, A. 1984, *Ap. J.*, **283**, 64.
Malin, D. F., and Carter, D. 1983, *Ap. J.*, **274**, 534.
Malkan, M. A., Margon, B., and Chanan, G. A. 1984, *Ap. J.*, **280**, 66.
Markarian, B. E. 1967, *Astrofizika*, **3**, 55.
Markarian, B. E., and Lipovetskii, V. A. 1974, *Astrofizika*, **10**, 307.
Markarian, B. E., Lipovetskii, V. A., and Stepanian, D. A. 1979, *Astrofizika*, **15**, 549.
Meurs, E. J. A., and Wilson, A. S. 1984, *Astr. Ap.*, **136**, 206.
Mirabel, I. F., and Wilson, A. S. 1984, *Ap. J.*, **277**, 92.
Noreau, L., and Kronberg, P. P. 1986, *A.J.*, **92**, 1048.
Norman, C., and Silk, J. 1983, *Ap. J.*, **266**, 502.
Osterbrock, D. E. 1984, *Quart. J.R.A.S.*, **25**, 1.
Rieke, G. H., and Low, F. J. 1975, *Ap. J. (Letters)*, **200**, L67.
Roos, N. 1981, *Astr. Ap.*, **104**, 218.
_____. 1985*a*, *Ap. J.*, **294**, 479.
_____. 1985*b*, *Ap. J.*, **294**, 486.
Sandage, A., and Brucato, R. 1979, *A.J.*, **84**, 472.
Sandage, A., and Tammann, G. A. 1981, *A Revised Shapley-Ames Catalog of Bright Galaxies* (Washington, DC: Carnegie Institution of Washington), p. 91.
Schinckel, A., and Phillips, M. 1983, *A Catalogue of Active Galaxies*, (Anglo-Australian Observatory), unpublished.
Sharp, N. A. 1986, *Ap. J.*, **302**, 245.
Simkin, S. M., Su, H. J., and Schwarz, M. P. 1980, *Ap. J.*, **237**, 404.
Stauffer, J. R. 1982, *Ap. J.*, **262**, 66.
Stockton, A. 1978, *Ap. J.*, **223**, 747.
_____. 1982, *Ap. J.*, **257**, 33.
Stockton, A., and MacKenty, J. W. 1983, *Nature*, **305**, 678.
_____. 1987, *Ap. J.*, **316**, 584.
Sulentic, J. W., and Tifft, W. G. 1973, *The Revised New General Catalogue of Nonstellar Astronomical Objects* (Tucson: University of Arizona Press).
Theys, J. C., and Spiegel, E. A. 1976, *Ap. J.*, **208**, 650.
Thompson, L. A. 1986, *Ap. J.*, **300**, 639.
Thuan, T. X. 1983, *Ap. J.*, **268**, 667.
Toomre, A., and Toomre, J. 1972, *Ap. J.*, **178**, 623.
Veron-Cetty, M. P., and Veron, P. 1984, *ESO Sci. Rept.*, No. 1.
Ward, M. J., and Wilson, A. S. 1978, *Astr. Ap.*, **70**, L79.
Watanabe, M., Kodaira, K., and Okamura, S. 1982, *Ap. J. Suppl.*, **50**, 1.
Weedman, D. W. 1977, *Ann. Rev. Astr. Ap.*, **15**, 69.
Wehinger, P. A., and Wyckoff, S. 1977, *M.N.R.A.S.*, **181**, 211.
Wilson, A. S., and Meurs, E. J. A. 1982, *Astr. Ap. Suppl.*, **50**, 217.
Wilson, A. S., and Ulvestad, J. S. 1982, *Ap. J.*, **260**, 56.
Wyckoff, S., Wehinger, P. A., and Gehren, T. 1981, *Ap. J.*, **247**, 750.
Yee, H. K. C. 1983, *Ap. J.*, **272**, 473.

JOHN W. MACKENTY: Space Telescope Science Institute, 3700 San Martin Drive, Baltimore, MD 21218